ANL/NDM-160

Fast Neutrons Incident on Rotors: — Tantalum

Nuclear Data and Measurments Series

Nuclear Engineering Division
Argonne National Laboratory

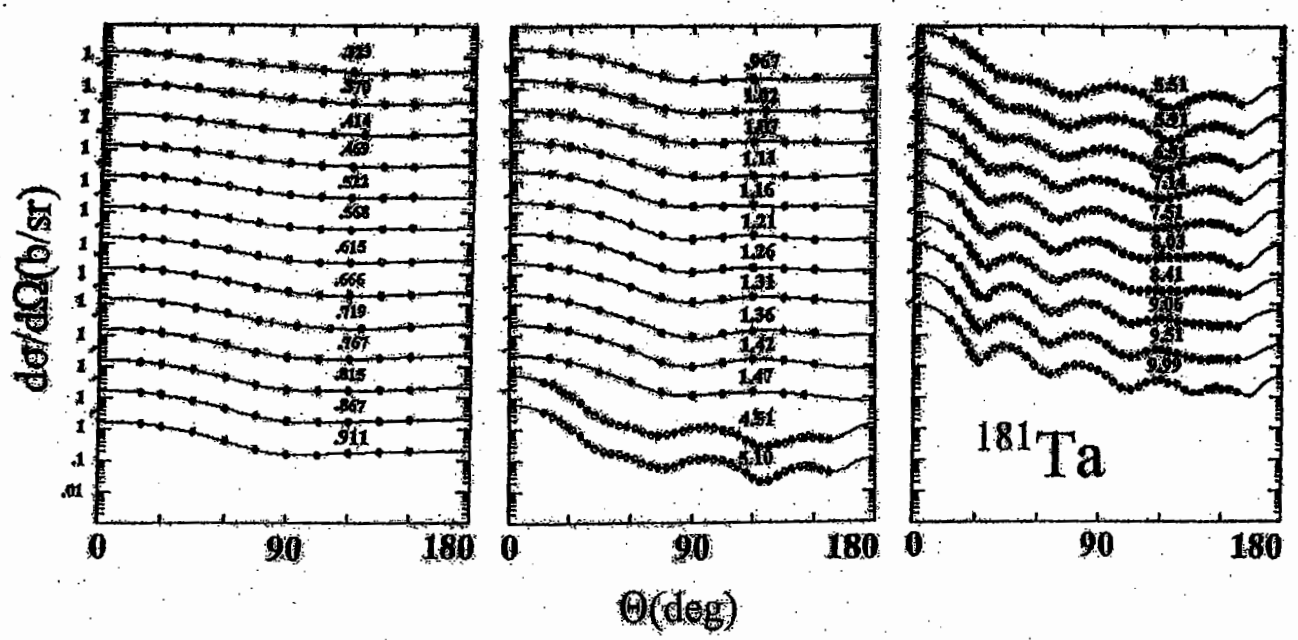

ARGONNE IS OPERATED BY THE UNIVERSITY OF CHICAGO FOR THE U.S. DEPARTMENT OF ENERGY OFFICE OF SCIENCE

Office of Science
U.S. DEPARTMENT OF ENERGY

THE UNIVERSITY OF CHICAGO

ARGONNE NATIONAL LABORATORY

About Argonne National Laboratory

Argonne is operated by the University of Chicago for the U. S. Department of Energy Office of Science, under contract W-31-109-ENG-38. The Laboratory's main facility is outside Chicago, at 9700 south Cass Avenue, Argonne, Illinois 60439. for Information about Argonne and its pioneering science and technology programs, see www.anl.gov.

Availability of This Report

This report is available, at no cost, at http://www.osti.gov/bridge. It is also available on paper to the U. S. Department of Energy, and its contractors, for a processing fee, from:

U. S. Department of energy
Office of Scientific and Technical Information
P.O. Box 62
Oak Ridge, TN 37831-0062
Phone (865) 576-6401
Fax (865) 576-5728
Reports@adonis.osti.gov.

Disclaimer

This report was prepared as an account of work sponsored by an agency of the United States Government. Neither the United States Government nor any agency thereof, nor the University of Chicago, nor any of their employees or officers, makes any warranty , express or implied, or assumes any legal liability or responsibility for the accuracy, completeness, or usefulness of any information, apparatus, product or process disclosed, or represents that its use would not infringe privately owned rights. Reference herein to any specific commercial product, process, or service by trade name, trademark, manufacturer, or otherwise, does not necessarily constitute or imply its endorsement, recommendation, or favoring by the United States Government or any agency thereof, Argonne National Laboratory, or The University of Chicago.

Nuclear Data and Measurement Series

Reports in the Argonne National Laboratory Nuclear Data and Measurement Series present results of studies in the field of microscopic nuclear data. The primary objective of the series is the dissemination of information in the comprehensive form required for nuclear technology applications. This series is devoted to: a) measured microscopic nuclear parameters, b) experimental techniques and facilities employed in measurements, c) the analysis, correlation and interpretation of nuclear data, and d) the compilation and evaluation of nuclear data. Contributions to this Series are reviewed to assure technical competence and, unless otherwise stated, the contents can be formally referenced. This Series does not supplant formal journal publication, but it does provide the more extensive information required for technological applications (e.g., tabulated numerical data) in a timely manner.

Publications in the ANL/NDM Series

A listing of recent issues in this series is given below. Issues and/or titles prior to ANL/NDM-130 can be obtained from the National Technical Information Service, U. S. Department of Commerce, Technology Administration, Springfield, VA 22161, or by contacting the author of this report at the Nuclear Engineering Division, Argonne National Laboratory, 9700 South Cass Avenue, Argonne, IL 60439 (USA). In addition, the entire report series can be found on the Internet at the following URL:

<http://www.td.anl.gov/reports/ANLNDMReports.html>,

including abstracts, complete reports, and associated computer programs.

A. B. Smith and P. T. Guenther
Fast-neutron interaction with the fission product ^{103}Rh
ANL/NDM-130, September 1993

A. B. Smith and P. T. Guenther
Fast-neutron scattering from vibrational Palladium nuclei
ANL/NDM-131, October 1993

A. B. Smith
Neutron interaction with doubly-magic ^{40}Ca
ANL/NDM-132, November 1993

A. B. Smith
Fast-neutron scattering at Z=50:- Tin
ANL/NDM-133, September 1994

A. B. Smith, S. Chiba and J. W. Meadows
An evaluated neutronic data file for elemental Zirconium
ANL/NDM-134, September 1994

A. B. Smith and S. Chiba
Neutron scattering from Uranium and Thorium
ANL/NDM-135, February 1995

A. B. Smith
Neutron scattering and models:- Iron
ANL/NDM-136, August 1995

A. B. Smith
Neutron scattering and models:- Silver
ANL/NDM-137, July 1996

A. B. Smith and D. Schmidt
Neutron scattering and models:- Chromium
ANL/NDM-138 June 1996

W. P. Poenitz and S. E. Aumeier
The simultaneous evaluation of the standards and other cross sections of importance for technology
ANL/NDM-139, September 1997

D. L. Smith and J. T. Daly
A compilation of information on the ^{31}P(p,gamma)^{32}S reaction and properties of excited levels in ^{32}S
ANL/NDM-140, November 2000

A. B. Smith
Neutron scattering and models:- Titanium
ANL/NDM-141, July 1997

A. B. Smith
Neutron scattering and models:- Molybdenum
ANL/NDM-142, July 1999

R. E. Miller and D. L. Smith
Compilation of information on the ^{31}P(p,gamma)^{33}Cl reaction and properties of excited levels in ^{33}Cl
ANL/NDM-143, July 1997

R. E. Miller and D. L. Smith
A compilation of information on the ^{31}P(p,gamma)^{28}Si reaction and properties of the excited levels in ^{28}Si
ANL/NDM-144, November 1997

R. D. Lawson and A. B. Smith
ABAREX, a neutron spherical optical-statistical model code:- A user's manual
ANL/NDM-145, June 1999

R. T. Klann and W. P. Poenitz
Non-destructive assay of EBR-II blanket elements using resonance transmission analysis
ANL/NDM-146, 1998

A. B. Smith
ELEMENTAL-ABAREX:- A user's manual
ANL/NDM-147, June 1999

D. G. Naberejnev and D. L. Smith
A method to construct covariance files in ENDF/B formats for critical safety applications
ANL/NDM-148, June 1999

A. B. Smith
Neutrons and antimony:- physical measurements and interpretations
ANL/NDM-149, July 2000

A. B. Smith and A. Fessler
Neutrons and antimony:- neutronic evaluations of ^{121}Sb and ^{123}Sb
ANL/NDM-150, July 2000

A. B. Smith
Fast neutrons incident on Holmium
ANL/NDM-151, December 2000

R. D. Lawson and A. B. Smith
Technical note:- Dispersion contributions to neutron reactions
ANL/NDM-152, August 2001

A. B. Smith
Fast-neutrons incident on Hafnium
ANL/NDM-153, June 2001

D. L. Smith, Dimitri G. Naberejnev and L. A. Van Wormer
An approach for dealing with large errors
ANL/NDM-154, September 2001

A. B. Smith
Fast-neutron scattering from elemental Rhenium
ANL/NDM-155, August 2003

D. L. Smith
A demonstration of the lognormal distribution
ANL/NDM-156, July 2003

A. B. Smith
Fast-neutrons incident on Gadolinium
ANL/NDM-157, April 2004

D. L. Smith
A survey of experimental and evaluated fast-neutron Helium production data for fusion applications
ANL/NDM-158, May 2004

D. L. Smith
Covariance matrices for nuclear cross sections derived from nuclear model calculations
ANL/NDM-159, January 2005

ANL/NDM-160

FAST-NEUTRONS INCIDENT ON ROTORS:- TANTALUM*

by

Alan B. Smith[a,b]
[a]Argonne National Laboratory, Argonne, Illinois; and
[b]The Physicist's Consultative, Ottawa, Illinois

February 2005

Keywords:-
Measured neutron scattering 0.3 – 10.0 MeV. Optical-statistical and coupled-channels model analysis of experimental results. Basic and applied physical comments. Regional model.

---

*This work supported by the United States Department of Energy under contract W-31-109-ENG-38.

TABLE OF CONTENTS

Abstract 7

I. Introductory Remarks 7

II. Experimental Methods 8

III. Experimental Results 9

IV. Physical Models

IV-A. Spherical Optical-Statistical Model (SOM) 10
IV-B. Coupled-Channels Rotational Model (ROTM) 14
IV-C. Dispersive Effects 17

V. Some Comparisons with Other Potentials and with ENDF/B-VI

V-A. Comparisons with Other Potentials and a Regional Model 19
V-B. Comparisons with the ENDF/B-VI Evaluated File 21

VI. Concluding Remarks 22

Acknowledgments 23

References 23

Appendices

A. Total Cross-Section Experimental Data Base 25
B. Prior Elastic-Scattering Data Base 26
C. Prior Inelastic-Scattering Data Base 27

Tables 29

Figures 35

ANL/NDM-160

FAST-NEUTRONS INCIDENT ON ROTORS:- TANTALUM

ABSTRACT

Mono-energetic neutrons are scattered from elemental tantalum over two incident-neutron energy ranges. The first set of data is distributed over E ≈ 0.3 – 1.5 MeV, including both elastic and inelastic processes. These results supplement those reported by the author and co-workers some time ago. The second set of data consists of detailed measurements over the energy range E ≈ 4.5 – 10.0 MeV. The present work is augmented with neutron scattering and total-cross-section data from the literature to form a composite experimental database. The latter is interpreted in the context of optical-statistical and coupled-channels models, including consideration of collective deformations, dispersive effects, and other physical properties. The results are compared with those of similar neutron interactions in this region of collective deformations. A "regional" model is proposed for the interpretation of such neutron interactions. The model and the experimental results are compared with relevant values given in ENDF/B-VI. Future work is suggested.

I. INTRODCUTORY REMARKS

Nuclei in the A ≈ 155 – 185 region are characterized by complex low-energy structure largely governed by collective rotational and/or vibrational motions. Most of these elements are multi-isotopic with asymmetries [(N-Z)/A] of ≈ 0.17 - 0.20. At relatively low incident energies the interaction of neutrons with these collective nuclei is very much influenced by the collective properties. Conversely, low-energy particles are sensitive probes for studying such structure. This is particularly true of fast (few-MeV) neutrons where the interaction is not inhibited by coulomb effects. Many of these nuclei are fission products with enhanced collective structure following from the fission process. Collective aspects of the interactions are prominent and should be incorporated in the "regional" models. Experimental and analytical studies of the fast-neutron interaction with collective nuclei in this region have been a prominent part of fast-neutron work at Argonne for the last several years (**Smi00**, Smith, 2000; **Smi01**, Smith, 2001; **Smi03**, Smith, 2003; **Smi04**, Smith, 2004). The present work is an additional aspect of these endeavors, from which an improved "regional" nuclear model is derived and presented here.

The subject of the present study is tantalum. It is essentially mono-isotopic (99.988% ^{181}Ta), and a complex rotational nucleus. The low-energy excited structure is governed be two single-particle states and their associated rotational bands (**MN59**, Mottelson and Nilsson, 1959; Preston, 1962; **NDS92**, Firestone, 1992; **Dra+98**, Dracoulis et al., 1998). This single particle and collective

structure can be described in the framework of the collective model. Assuming a deformation of $\delta \approx 0.3$, such calculations attribute the 73rd proton to $9/2^-[514]$ or $5/2^+[402]$ configurations. However, the $7/2^+[404]$ and $9/2^-[514]$ configurations are energetically very similar and pairing effects can result in the former having the lower energy. This is apparently the case in tantalum as observations show the ground state is the $7/2^+[404]$ configuration and the first-excited state, at only ≈ 6.2 keV, the $9/2^-[514]$ configuration. Each of these collective states has clearly evident rotational bands that comprise most of the tantalum structure to excitations of ≈ 1.0 MeV and above. The same theoretical model also predicts the single-particle configurations $5/2^+[402]$ and $1/2^+[411]$ at somewhat higher excitation energies. The band heads of these latter structures may be represented by the levels reported at excitations of 482 and 615 keV, respectively, however associated rotational band structure has not been clearly identified. That question remains a potential for future structure studies. While there are some structure uncertainties, it is evident that the present "scattering" measurements and their interpretations are very largely governed by well-known components of the first two rotational bands.

Tantalum is a heavy, high-temperature and non-corrosive metal that has a potential for application in a diversity of special nuclear endeavors, and collective nuclei in this region are common fission products. This study, and early work by the author and his associates, provides the majority of the experimental and calculational knowledge of the fast neutron scattering from tantalum. This may be of practical importance as the current evaluated tantalum data file (**ENDF/B-VI**) used in applied design calculations is now more than thirty years old and based upon fragmentary experimental information (see **Appendices**) and/or antiquated models. It is an objective of this document to report extensive new experimental information and model results relevant to this important collectively-deformed mass region.

II. EXPERIMENTAL METHODS

All of the neutron scattering measurements reported here employed the fast-neutron time-of-flight technique (**CL55**, Cranberg and Levin, 1955). The early work of Smith and coworkers (**Smi+63**, Smith et al., 1963; **Smi+68**, Smith et al., 1968), and the additional work below incident neutron energies of ≈ 1.5 MeV reported here, employed essentially the same apparatus and techniques. The neutron source was the ^{7}Li(p,n)^{7}Be reaction (**Dro87**, Drosg, 1987) producing both a primary and a secondary neutron group. The latter distorted inelastic-scattering results near excitations of ≈ 0.5 MeV. The lithium target was a metal film with its thickness and the energy of the incident proton beam adjusted to provide neutrons incident on the scattering sample with energy spreads of $\approx 20 - 30$ keV. The incident proton beam was pulsed and bunched using a magnetic system (**Mob77**, Mobley, 1977) so as to provide proton (i.e. neutron) bursts of ≈ 1 nsec duration at a 1 MHz repetition rate. The scattering sample used in all of the measurements was a 2 cm. diameter 2 cm. long cylinder of high-purity elemental tantalum metal placed ≈ 12 cm from the neutron source at a zero-degree reaction angle. Eight heavily shielded, angle-adjustable, flight paths of ≈ 2 m. length were arranged about the sample. The measured scattered-neutron angular distributions consisted of eight or more differential values at each energy, distributed between ≈ 20 and 160 deg. The neutrons were detected using 5 cm. diameter

hydrogenous liquid scintillaters with pulse-shape-sensitive circuitry to suppress background gamma rays. The scattered-neutron energy resolution of the spectrometer was ≈ 30 - 40 keV at these lower energies. Another time-of-flight system monitored the relative neutron-source intensity. The relative scattering angles were determined to ≈ 0.1 deg. with precision optical instruments. The absolute normalization of the relative angular scale was then determined to ≈ 1.0 deg. by observing the energy shift of neutrons scattered from a CH_2 (polyethylene) scatterer to either side of the apparent angular centerline. The relative energy-dependent responses of the detectors were determined by observation of the "prompt" neutrons emitted at the spontaneous fission of ^{252}Cf, as described by Smith et al. (**SGS77,** Smith, Guenther and Sjoblum, 1977). These relative responses were then normalized by observation of neutron scattering from primarily carbon, or in a few instances from zirconium, as given by Lane et al. (**Lan+61**, Lane et.al., 1961).

The second portion of the present measurements was at incident-neutron energies of ≈ 4.5 - 10.0 MeV. For this part of the work the number of the above flight paths was increased to 10 and each was extended to approximately a 5 m. length. The neutron source was changed to the D(d,n)^{3}He reaction (**Dro87,** Drosg, 1987), with the deuterium target gas contained in a 2.5 cm. long cell at a pressure of two atmospheres. The incident deuterons were pulsed at a 1 MHz rate and klystron bunched to ≈ 1 nsec. duration. The scattered-neutron detector radii were increased to 12.7 cm. The angle calibration was the same as for the above low-energy measurements. Again, the relative energy responses of the detectors were determined by the observation of fission neutrons from the spontaneous fission of ^{252}Cf, and the absolute detector normalizations were determined by the measurement of scattering from the well-known scattering standard H(n,n) (**CSL83**, Conde, Smith and Lorenz, 1983) using a polyethylene sample.

All of the scattering measurements were corrected for angular resolution, beam attenuation and multi-event effects using Monte-Carlo techniques (**Smi91,** Smith, 1991). More extensive discussion of the methods employed in this work is found in a number publications [e.g. (**SG92**, Smith and Guenther, 1992; **Chi+92**, Chiba et al., 1992; **Bud+82**, Budtz-Jorgensen et al., 1982; **Smi+67,** Smith et al., 1967; and references cited therein).

III. EXPERIMENTAL RESULTS

The experimental results are presented here in two parts. The first, Part-A, extends over the incident-neutron energy range of ≈ 0.3 – 1.5 MeV and the second, Part-B, extends over the incident enegy range of ≈ 4.5 – 10.0 MeV. Both Parts of the data were obtained using fundamentally the same techniques differing only in detail, as outlined in **Sec. II**, above.

Part-A data consists of approximately 130 differential "elastic" distributions and a lesser number of inelastic distributions. Approximately 15% of these "elastic" distributions were reported many years ago (**Smi+63,** Smith et al., 1963). A few years later another approximately 50% of the results of Part-A were reported (**SGW68**, Smith, Guenther and Whalen, 1968). The remainder of the results of Part-A was obtained over more recent years, and are reported here for

the first time. The inelastic-scattering results are relatively sparse, and will be dealt with in the model discussions of **Sec. IV-B**. The "elastic" angular distributions were distributed approximately uniformly over the incident energy range E ≈ 0.3 - 1.5 MeV. There are a large number of distributions that would be difficult to individually deal with in the modeling, and the quality varied. Therefore these lower-energy "elastic" distributions were binned over ≈ 50 - 60 keV incident-energy intervals and averaged using the individual legendre-polynomial expansions to interpolate in angle, and weighting by the estimated uncertainties. The resulting averaged distributions extended from E ≈ 0.32 - 1.47 MeV, with approximately ten differential cross-section values per distribution distributed between ≈ 20 and 150 deg. These averaged measured "elastic"-scattering distributions are shown in **Fig. III-1**, together with the results of legendre-polynomial fitting of the experimental quantities. The uncertainties of the averaged differential values were taken to be 5%, or the RMS values following from the averaging procedure, whichever was larger. The scattered-neutron energy resolutions varied, as discussed in **Sec. IV**.

Part-B experimental data consists of twelve distributions approximately evenly spaced over the incident energy range E ≈ 4.5 - 10.0 MeV. The experimental scattered-neutron resolution was approximately 350 keV so each distribution contains a considerable inelastically-scattered component, as discussed in **Sec IV**, below. Every distribution consisted of approximately forty differential values distributed between ≈ 20 and 160 deg. The total uncertainties were constructed from the statistical and systematic contributions of the present measurements, and ranged from several percent to more than ten percent at the extreme minima of some of the distributions. These Part-B results are also shown in **Fig. III-1,** together with the corresponding legendre-polynomial representations.

IV. PHYSICAL MODELS

IV-A. Spherical Optical-Statistical Model (SOM)

As noted in the introductory remarks, tantalum is far from a spherical or "near spherical" nucleus whose interaction with incident fast neutrons can be quantitatively described in terms of the conventional spherical optical-statistical model (**Fes58,** Feshbach, 1958; **Hod63,** Hodgson, 1963; **FPW54**, Feshbach, Porter and Weisskopf, 1954; **Wol51**, Wolfenstein, 1951). There are compound-nucleus and direct-reaction aspects of the neutron interaction with tantalum. The latter are usually described with the coupled-channels formalism. Despite these complications, the conventional SOM has wide basic and applied use, and it does conserve canonical variables such as energy, angular momentum, spin and parity. Because of this applicability a number of "spherical" and "near spherical" global and regional optical models have been presented in the literature over the years, with generally increasing success and improved predictability. One of the more recent of these is that of Koening and Delaroche (**KD03,** Koening and Delaroche, 2003). The present SOM investigations were undertaken in the spirit of an approximation of potential usefulness in this region of collective deformation, and for initial guidance of the more appropriate coupled-channels concepts discussed below.

Throughout all of the physical modeling of the present work it was assumed that the real potential had the Saxon-Woods form and the imaginary potential the Saxon-Woods-Derivative form. A real spin-orbit potential of the Thomas form was used with the parameters of Walter and Guss (**WG85**, Walter and Guss, 1985). There was no imaginary volume potential, as the considerations were at relatively low energies, and there was no imaginary spin-orbit potential. The geometric shapes of these potentials are defined by Hodgson (**Hod63**, Hodgson, 1963), among many others. Compound nucleus processes were considered with resonance width-fluctuation and correlation corrections in the manner of Moldauer (**Mol80**, Moldauer, 1980). The ground and fourteen discrete excited states in tantalum up to excitations of 1.028 MeV were explicitly considered, using the energies, spins and parities given in the Nuclear Data Sheets (**NDS92**, Firestone, 1992). Higher-energy excitations were treated using the statistical continuum model and parameters of Gilbert and Cameron (**GC65**, Gilbert and Cameron, 1965). Neutron radiative-capture and neutron-induced charged-particle-emission processes were assumed to be negligible in the context of the present considerations, and ignored. All the SOM calculations were carried out with the calculational code ABAREX (**LS99**, Lawson and Smith, 1999).

The present SOM parameter derivations included consideration of the energy-averaged total cross sections at the energies of the "elastic"-scattering distributions (between ≈ 0.32 and 15.2 MeV). Calculated and measured total cross section comparisons extended upward to 20 MeV. The energy-averaged total cross sections are consistent with the energy-average concepts of the SOM. Partially resolved resonance fluctuations may persist at very low energies that are well below those of the present considerations. The total cross sections used in the fitting are those defined in **Appendix A** and illustrated in **Fig. A-1**. The differential elastic-scattering cross sections used in the SOM derivations included all those of the present work (as summarized in **Fig. III-1**) plus those found in the literature, as summarized in **Appendix B**. The composite elastic-scattering database, extending from 0.323 to 15.2 MeV, was inspected and a few distributions from the literature abandoned as being grossly inconsistent with the body of experimental information. The final 54 "elastic"-scattering distributions of the database are illustrated in **Fig. IV-A-1** and **Fig. IV-A-2** (identical experimental data are shown in both figures). This "elastic"-scattering database is relatively strong from ≈ 0.3 - 1.5 MeV and from 4.5 - 10.0 MeV. There is very little information between these two energy intervals, and what there is can be questioned. There are five distributions between ≈11.0 and 15.2 MeV, and no experimental scattering information above ≈ 15.2 MeV what so ever. All of these "elastic" distributions certainly include inelastic-scattering contributions due to the excitation of the first-excited (6.2 keV) level. It is not technologically feasible to experimentally resolve these two scattered components. In some cases considerably more inelastic contamination is included in the measured "elastic" distributions due to excitation of higher-lying levels and lesser experimental resolution. The scattered-neutron resolutions are reasonably known for the present measurements. All those up to ≈ 1.1 MeV include only elastic and first-inelastic components. For incident energies of ≈ 1.1 - 1.5 MeV some of the present measured results are estimated to include the elastic component plus inelastic contributions from the excitation of ≈ 6, ≈ 136 and ≈158 keV levels. Above incident energies of ≈ 4.5 MeV the present "elastic" results include

inelastic contributions due to the excitation of levels up to and including the 338 keV state. All of the SOM calculations explicitly considered these inelastically-scattered contaminates assuming the respective interactions were due to compound-nucleus processes.

The SOM parameters were obtained by least-square fitting the above neutron total and "elastic"-scattering database. The initial fitting followed through six sequential steps, first determining the real potential diffuseness (a_v), then progressively the reduced real-potential radius (r_v, where $r_i = r_i \cdot A^{1/3}$), the imaginary reduced radius (r_w), the imaginary diffuseness (a_w), the real-potential strength (V) and the imaginary-potential strength (W). The uncertainties of the differential data were taken as noted above for the present data, or as given by the various authors. When not available or qualitatively suspicious, the uncertainties were estimated by the present author. The weights of the total cross sections were increased in the fitting procedures so as assure that the total cross sections would have some impact. Various total cross section weights were examined ranging from zero (no effect) to the equivalent of 20 differential values. After a number of attempts it was felt that a total cross section weight making the value equivalent to that of 5-10 differential "elastic"-scattering values at each energy was most appropriate and was adopted for the majority of the final fitting. It became evident that the full six-parameter fitting procedure did not lead to very stable SOM parameters, particularly those associated with the imaginary potential. Furthermore, the resulting imaginary diffusenesses, though not well determined, were abnormally small. The same type of behavior has been observed in SOM fitting of the similarly deformed, collective isotopes of rhenium and gadolinium. (**Smi03**, Smith, 2003; **Smi04**, Smith, 2004). Therefore, the real and imaginary diffusenesses were fixed to the values found suitable for rhenium or for gadolinium, and the tantalum fitting repeated using four-parameter searches, progressively determining real and imaginary potential radii and the real and imaginary strengths V and W. This approach led to more stable parameters, though the imaginary potential still tended to be unusual, but similar to SOM potentials previously observed in this deformed mass region. The SOM potential parameters obtained with the two alternate sets of diffusenesses are given in **Table IV-A-1** and **Table IV-A-2**.

The total cross sections calculated with both of the above potentials are in reasonably good agreement with averages of the measured values up to more than 20 MeV, as illustrated in **Fig. IV-A-3**, despite the fact that the two potentials are quite different in real and imaginary strengths and radii. Differences between measurements and calculations are several percent or less, probably smaller than the experimental uncertainty and certainly smaller than the differences between individual experimental data sets. The calculated values tend to be several percent smaller than the averages of the measured values in the 1 - 5 MeV region. However, the measurements alone show fluctuations in this region that are not consistent with the energy dependence of a SOM. Moreover, this is an energy region where there are only several experimental "elastic" distributions to guide the model development. Panel B of **Fig. IV-A-3** shows a slight irregularity in the calculated results near five MeV, reflecting the linear approximations used in representing the imaginary potential of **Table IV-A-2**. The total cross sections obtained with the SOM and the parameters of **Table IV-A-1** seem marginally superior

to those obtained with the parameters of **Table IV-A-2.** Both of the above SOM potentials yield S_0 strength functions of $\approx 3.4 \times 10^{-4}$ compared to the experimentally-deduced value of 1.7 (± 0.12) x 10^{-4} (**Mug+81**, Mughabghab et al., 1981). This difference is not surprising as tantalum is in a deformed mass region where the SOM is known to over-predict the measured S_0 strength functions. The predicted SOM S_1 strength functions are also larger than deduced from measurements, particularly so for the potential of **Table IV-A-2** which has an unusual low-energy imaginary-potential behavior.

Measured and SOM-calculated differential scattering cross sections are compared in Figs. **IV-A-1** and **IV-A-2.** The calculations of the first of these figures are based upon the potential of **Table IV-A-1** using Gd diffusenesses, and are the better of the two representations. These examples illustrate the rather general problems that haunt derivations of the SOM in this region of strong collective effects. The description of the observed angular distributions up to approximately 1.5 MeV is fairly good. This suggests that the experimental resolutions of the measured data are a reasonably estimate. The sparse experimental data between 2 – 4 MeV (four distributions) is only marginally described. This data came from one measurement set, other aspects of which have demonstrated some problems. An attempt was made to fit the overall data without using the 1.5 - 4.5 MeV energy range. The resulting potential parameters were not greatly different from those obtained using the entire database. From 4.5 - 10.0 MeV the SOM of **Table IV-A-1** gave qualitative reasonable differential results. There is a trend for the SOM to underestimate the cross sections in the defraction minima of the distributions by relatively large amounts. This is to be expected, as it is in such regions that the direct processes, not considered by the SOM, make a strong contribution. There are five measured distributions distributed between 11.0 and 15.2 MeV. The SOM of **Table IV-A-1** describes them with varying degrees of success. Again, the calculated minima of the distributions are notably smaller than the observed values. The experimental-calculational comparisons of **Fig. IV-A-2** are similar to those of **Fig. IV-A-1**, except at the highest energies where the agreement between measurement and calculation tends to deteriorate at large angles. It was noted that the details of the SOM absorption are very sensitive to collective effects. It was also noted that these reasonably successful SOM representations of the neutron interaction with tantalum result in a relatively small imaginary strength, particularly a very narrow surface-absorption width. This seems to be characteristic of SOM potentials deduced from neutron data in this highly collective region. Similar behavior has been noted in dealing with rhenium and gadolinium (**Smi03,** Smith, 2003; **Smi04**, Smith, 2004).

The SOM real potential radii tend to be smaller than global trends which impacts upon the real-potential strength through the well-known Vr correlation of real radius and strength. Furthermore the energy dependence of the real strength in this collective region seems to be erratic and dependent upon choice of imaginary potential (compare **Tables IV-A-1** and **IV-A-2**). SOM potentials are a practical parameterization of the neutron interaction with collectively-deformed targets but they should not be used as indicators of physical properties such as implied by the non-locality of the nuclear force (**PB62**, Perey and Buck, 1965; **Bau+82,** Bauer et al., 1982).

IV-B. Coupled-Channels Rotational Model (ROTM)

As afore said (**Sec. I**), tantalum is essentially a monoisotopic element whose low-lying structure is defined by two or more collective rotational bands. The incident neutron strongly interacts with the members of these collective bands in a manner inconsistent with the concept of a spherical optical-statistical model. Better is the Distorted-Wave Born Approximation (DWBA), and still better is the coupled-channels model (**Tam65**, Tamura, 1965). In the present endeavor the latter method was used assuming a $7/2^+$[404] g.s. rotational band. The first three levels of this band (g.s. $7/2^+$, 0.136 keV $9/2^+$ and 0.302 keV $11/2^+$) were coupled with the incident neutron, assuming that $\beta_2 = 0.269$ and $\beta_4 = -0.090$ (**Kon04**, Kondev, 2004: **NDS92**, Firestone, 1992; **Dra+98**, Dracoulis et al., 1998). Members of the second 9/2[514] band (band head at 6.2 keV) were treated as conventional compound-nucleus contributions. These two bands result in 15 discrete states to $E_x \approx 1.1$ MeV, analogous to the compound-nucleus excitations outlined above in the context of the SOM. This is, of course, a first approximation for a very complex collective rotational interaction between the incident neutron and the target nucleus due to the close proximity of at least two low-lying ([404] and [514]) rotational bands. There are doubtless significant interactions between the incident neutron and other collective structures. However, their introduction would very much increase the complexity of the calculations, well beyond a definition reasonably achievable from an interpretation of the available experimental data.

The ROTM parameters were determined by least-square fitting the same 54 scattering distributions used in the above SOM derivations. The calculations were again arranged to include the effects of experimental resolutions as could be best estimated. For the present measurements it was clear that the inelastic scattering due to the excitation of the 6.2 keV level was included in all the measured "elastic" distributions up to incident energies of ≈ 1.0 MeV. For incident energies of ≈ 1.0 to 1.6 MeV, some of the present values were assumed to include components due to inelastic excitations of less than ≈ 160 keV, and above 1.6 MeV were assumed to include inelastic contributions due to the excitation of all levels below ≈ 350 keV. However, these are only qualitative estimates of the resolution of data taken from the literature, as the energy resolution is usually not well known. Clearly, the contributions from the inelastic excitation of the 6.2 keV level are included with the "elastic" scattering in all measurements. Resolution uncertainties were not a particular concern at incident energies of < 1.5 MeV as the database is dominated by the results of the present work. The same is true for incident energies of ≈ 4.5 to 10.0 MeV. There are only five reported "elastic" distributions above incident energies of 10 MeV (at ≈ 11.0 - 15.2 MeV). In this region compound-nucleus effects will be small but direct inelastic processes remain a resolution concern. The primary region of resolution uncertainties is again from ≈ 1.5 to 4.5 MeV where there are only four experimental "elastic" distributions. In addition, data comparisons and fitting suggest some problems with several of the reported experimental distributions from the literature near incident energies of 5.0 MeV. Where results were obviously anomalous, they were abandoned.

All of the ROTM calculations utilized versions of the computational code ECIS94 (**Ray94**, Raynal, 1994). The calculations included compound-nucleus and continuum neutron emission processes with parameters identical to those of the above SOM calculations. However, the neutron total cross sections were not included in the fitting procedures, as in the SOM interpretations, but were compared with the calculated results after the fitting to guide the parameterizations. After extensive fitting it became clear that the ROTM geometric parameters were very similar to the "regional" parameters previously given by the author (**Smi04**, Smith, 2004), and they were accepted for subsequent fitting to determine the potential strengths. The resulting tantalum ROTM is given in **Table IV-B-1**. Those parameters result in a good description of the neutron total cross sections as illustrated in **Fig. IV-B-1**, and extrapolate to moderately higher r energies. The measured and calculated neutron total cross sections agree to within the experimental uncertainties alone.

The ROTM of **Table IV-B-1** is also reasonably descriptive of the measured "elastic" scattering distributions, as shown in **Fig. IV-B-2**. This figure represents the calculated results with three curves at each energy, corresponding to different resolution assumptions. The first (i) and lowest magnitude of these corresponds to the calculated elastic distribution plus inelastic contributions due to the excitation of the 6.2 keV level. The next two curves denote (ii) elastic plus inelastic contributions due to the excitation of all levels up to $E_x \approx 160$ keV, and curve (iii) elastic plus inelastic contributions due to the excitation of all levels up to $E_x \approx 360$ keV. Thus, these three curves reflect the reasonably assumed resolutions of the experimental measurements at the various energies. Curve (i) generally best represents the measured data up to incident energies of ≈ 1.0 MeV. Curve (ii) is arguably more suitable for incident energies of ≈ 1.0 to 4.0 MeV. Curve (iii), combining the two increments of inelastic scattering with the "elastic" component, is certainly most appropriate above 4.0 MeV. These comparisons support the resolutions estimated for the present measured differential data. Comparing the scattering distributions of **Fig. IV-B-2** with those of either **Figs. IV-A** or **IV-A-2**, it is clear that the ROTM provides a far more realistic description of neutron "elastic" scattering from tantalum than the SOM. This is particularly so in the minima of the distributions at higher energies.

Concurrent with the present "elastic"-scattering measurements, inelastic scattering cross sections were determined. These were all at incident energies of less than 1.6 MeV, and largely relevant to excitations of less than 0.6 MeV. The present inelastic cross sections were combined with those of the earlier work (**SGW68**; Smith, Guenther and Whalen, 1968) to form a composite experimental database. There seems to be essentially no other relevant experimental inelastic-scattering data (see **Appendix C**). The present composite data base was sorted into six inelastically-scattered groups, corresponding to experimentally observed excitations of:- 1) 139 keV (136 $9/2^+$, 158 $11/2^-$), 2) 316 keV (301 $11/2^+$, 337 $13/2^-$), 3) 499 keV (482 $5/2^+$, 495 $13/2^+$, 542 $15/2^-$), 4) 614 keV (615 $1/2^+$, 619 $3/2^+$), 5) 756 keV (716 $15/2^+$, 773 $17/2^-$) and 6) 870 keV (964 $17/2^+$, 1027 $19/2^-$), where the parenthetical quantities are the estimated contributions to the various observed groups from excited levels as cited in the Nuclear Data Sheets (**NDS92**, Firestone, 1992). The sixth of these observed groups is speculative and not well correlated with known excited structure. As afore said, the measurement of the inelastic-neutron excitation of the

first-reported level at 6.2 keV is not technologically feasible. It has also been noted that the observation of the third inelastically-scattered neutron group ($E_X \approx 499$ keV) is distorted by the second neutron group from the $^7Li(p,n)^7Be^*$ neutron-source reaction. Corrections were made for this source perturbation, but they introduced additional uncertainty. The sixth of the experimental excitations is speculative and not well correlated with reported excited structure. In total, there were several hundred angle-integrated inelastic-excitation cross sections from the present and previous work by the author and associates (**SGW68**, Smith, Guenther and Whalen, 1968; **Smi+63**, Smith et al., 1963). Those within each of the above observed inelastic groups were averaged over 100 keV incident-neutron energy intervals in order to reduce the experimental fluctuations. These averaged experimental results are shown in **Fig. IV-B-3**. Generally, the cross-section uncertainties are 10-20%, including estimates of resolution and systematic effects. The calculations coupled the first three levels of the g.s. rotational band, as described above. For these states the calculated inelastic cross sections consist of both direct and compound-nucleus components. The calculated results for all other discrete inelastic-scattering cross sections consist only of compound-nucleus contributions. The calculated and measured inelastic-scattering results are compared in **Fig. IV-B-3**. This figure also shows the calculated excitation of the 6.2 keV level for completeness. The calculated and measured excitations of the observed 139, 316 and 499 keV states are in reasonably good agreement. However, the calculated results are far smaller than the measured quantities for the excitation of the observed 614 and 756 keV levels. The same trends were observed in the previous work (**SGW68**, Smith, Guenther and Whalen, 1968). The levels contributing to these two excitations, as reported in the Nuclear Data Sheets (**NDS92**, Firestone, 1992), consist of only two levels for each of the observed excitations. The reported level distributions do not lead to inelastic cross-section magnitudes due to compound-nucleus processes anywhere near the magnitudes of the corresponding observed values. These comparisons suggest that something is wrong with; a) the measured values, b) the definition of the contributing excited structure, c) the assumed reaction mechanism (compound-nucleus), or d) the calculational mechanism— or all four factors may be contributing. As noted in the beginning, tantalum has a very complex excited structure consisting of at least 3-4 collective rotational bands. The levels of such bands are not entirely consistent with those cited in the Nuclear Data Sheets (**NDS92**, Firestone, 1992), nor with the results of recent particle-fusion studies (**Dra+98**, Dracoulis et al., 1998). Furthermore, the reported tantalum level density in the 0.5 to 1.0 MeV excitation region is odd, having far fewer states than is suggested by a reasonable statistical model (e.g. **GC65**, Gilbert and Cameron, 1965). The present experimental results and these factors suggest that there is a problem with the level specification as given in the Nuclear Data Sheets. There should be a number of additional levels in the region in question. With the complex collective structure of the tantalum target, the present model assuming coupling within the g.s. rotational band and simple compound-nucleus reactions otherwise may be a gross over simplification of the actual reaction mechanism. Far more complex couplings may well be present but they are unknown, and the experimental results are not definitive enough to define such complex assumptions. There is, of course, the possibility that there is a calculation error in the modeling. However, identical test problems were set up and results calculated with the SOM code ABAREX (**LS99**, Lawson and Smith, 1999) and the ROTM code ECIS94 (**Ray94**, Raynal, 1994). With no deformation, the respective results

were essentially identical. This suggests that the present inelastic concerns are not due to mechanical calculational error. Reasonable changes in β_2 will alter the calculated inelastic-scattering results but not by enough to alleviate the above discrepancies.

IV-C. Dispersive Effects

Dispersive effects can significantly impact on optical-model parameters as they inter-relate the real and imaginary potentials and reflect causality (**JLM77**, Jeukenne, Lejeune and Mahaux, 1977; **Lan62**, Lane, 1962; **Sat83**, Satchler, 1983; **Lip66**, Lipperheide, 1966; **Pas67**, Passatori, 1967; and, **Fes58**, Feshbach, 1958). These effects can be expressed in the form,

$$J_V(E) = J_{HF}(E) + (P/\pi) \cdot \int [J_W(E') / (E-E')] \cdot dE', \qquad \textbf{Eq. IV-C-1}$$

where J_V is the strength of the real potential, J_{HF} that of the local-equivalent Hartree-Fock potential, and J_W the strength of the imaginary potential. "P" denotes the principle value of the integral, which is evaluated from $-\infty$ to $+\infty$. Here, and throughout this section, potential strengths are given as volume-integrals-per-nucleon unless otherwise stated. The above integral can be broken into surface, ΔJ_{sur}, and volume, ΔJ_{vol}, components

$$\Delta J_{sur}(E) = (P/\pi) \cdot \int [J_{sur}(E') / (E-E')] \cdot dE' \qquad \textbf{Eq.. IV-C--2}$$

and

$$\Delta J_{vol}(E) = (P/\pi) \cdot \int [J_{vol}(E') / (E-E')] \cdot dE'. \qquad \textbf{Eq. IV-C-3}$$

With these equations, $J_V(E) = J_{eff}(E) + \Delta J_{sur}(E)$ and $J_{eff}(E) = J_{HF}(E) + \Delta J_{vol}(E)$, where $J_{sur}(E)$ and $J_{vol}(E)$ are surface- and volume-imaginary strengths, respectively. In the context of the present interpretations and with reasonable assumptions as to volume absorption, J_{HF} and ΔJ_{vol} are both approximately linear functions of energy thus the individual components can not be deduced from the experimental interpretations. The effect of **Eqs. IV-C-2** and **IV-C-3** is to add a surface and a volume component to the real potential that are some fractions of the imaginary surface and volume potentials. In the present work the magnitude of this contribution was calculated using the methods of Lawson and Smith (**LGS87**, Lawson, Guenther and Smith, 1987; **LS01,** Lawson and Smith, 2001). The latter reference gives a detailed description of the theory and method, and provides a FORTRAN code for executing the respective calculations. The method of Lawson and Smith (**LS01,** Lawson and Smith, 2001) requires a large energy extrapolation as there is only total cross section information above 15.2 MeV and the present potentials are shown to reasonably extrapolate to only $\approx$ 20 MeV. In particular, there is no guidance as to possible contributions from volume absorption or changes in imaginary-potential shapes with increasing energies. Moreover, the above integrals extend from $-\infty$ to $+\infty$ and thus some assumption as to the wide energy dependence of the respective parameters must be made.

The $\Delta J_{sur}(E)$ of **Eq. IV-C-2** is a surface strength to be added to the real potential. It is

assumed in the present application that the geometry of this contribution takes the same Saxon-Woods-Derivative form and associated geometric parameters as the imaginary surface absorption. It is further assumed that the $\Delta J_{vol}(E)$ retains the same Saxon-Woods geometry over all energies. These geometric assumptions are commonly used but they are just that, assumptions. Alternative energy-dependent shapes will be discussed elsewhere (**Smi05**, Smith, 2005). It was further assumed that the absorption was entirely a surface effect up to 20 MeV, in accord with the present model interpretations. It was then assumed to linearly fall with energy to zero at 80 MeV. Concurrently, a volume absorption was assumed to rise linearly from a zero value at 20 MeV to 80 MeV where it was given a strength the same as the surface-absorption strength at 20 MeV, and was then taken to be constant on to infinity. The imaginary potential was assumed to be zero at the Fermi Energy (E_F), to have a quadratic energy dependence from E_F to zero energy, and to be symmetric in energy about the Fermi Energy. E_F was taken to be – 6.822 MeV as determined from the mass tables (**Tul90**, Tuli, 1990). These assumptions are described in detail by Lawson and Smith (**LS01**, Lawson and Smith, 2001).

Following the above procedures and assumptions, $\Delta J_{sur}(E)$ of **Eq. IV-C-2** was calculated using the SOM of Table **IV-A-1**, and the ROTM of **Table IV-B-1**. There were a number of iterations, using two parameter fitting with the geometries fixed to that of rhenium (**Smi03**, Smith, 2003) for the SOM, and to that of the "regional" potential of Smith (**Smi04**, Smith, 2004) for the ROTM. These geometries were found to be very suitable, and restricting the fitting to two parameters made the treatment of a large number of iterations practical. These calculations determined the contribution of the imaginary SOM and ROTM potentials that is reflected into the real potential as a result of dispersion effects as a function of incident energy. An example of the fraction of the surface imaginary strength that is reflected into the real potential as a surface component is illustrated in **Fig. IV-C-1**. This particular example was deduced from the SOM potential after several iterations. Similar energy-dependent shapes were obtained with the ROTM but magnitudes are dependent on iteration and potential. This fraction falls from appreciable values at zero incident energy to essentially zero at ≈ 12 MeV and then becomes negative. The general overall behavior is illustrated by Lawson and Smith (**LS01**, Lawson and Smith, 2001). The iterative procedures were pursued through a number of cycles, finally resulting in the dispersive SOM and ROTM model parameters given in **Tables IV-C-1** and **IV-C-2**. These potentials result in reasonably good representations of the measured neutron total cross sections up to 20 MeV and beyond, as illustrated in **Fig. IV-C-2**. Panel "A" of that figure compares the measurements with the results of dispersive SOM calculations. The result is comparable to that obtained with the simple SOM calculations illustrated in **Fig. IV-A-3.** The same conclusion applies to the ROTM calculations of total cross sections as is evident from a comparison of **Figs. IV-B-1** and Panel "B" of **Fig. IV-C-2**. These general conclusions are true of comparisons of measured and calculated differential-scattering cross sections obtained with the SOM and the ROTM with and without dispersive effects as is evident from comparisons of **Fig. IV-C-3** with **Figs. IV-A-1**, and of **Fig. IV-C-4** with **Figs. IV-B-2**.

V. SOME COMPARISONS WITH OTHER POTENTIALS AND WITH ENDF/B-VI

V-A. Comparisons with Other Potentials and a Regional Model

Over recent years there have emerged a number of coupled-channels models for describing the interaction of fast neutrons with nuclei in this collectively-deformed region of A ≈ 150 – 200, largely as the result of work at Los Alamos (**YA87**, Young and Arthur, 1987) and Argonne. The target nuclei are both collective vibrators and rotators, with the nuclear asymmetry increasing from ≈ 0.160 to 0.200 and β_2 quadrupole deformations in the range of ≈ 0.15 – 0.30. These potentials were summarized and a "regional" potential constructed from them by Smith (**Smi04**, Smith, 2004). The present work augments these models as summarized in **Table V-A-1(A)** where the real- and imaginary- potential strengths are tabulated in terms of volume-integrals-per-nucleon for each of the target nuclei. These strengths and energy dependencies are remarkably consistent, showing no clear dependence on asymmetry [(N-Z)/A = η], deformation (β_2), target mass (A) or target charge (Z). Generally, the real-potential strengths decrease with energy from about $J_V \approx 442$ at E = 0.0 MeV at a rate of ≈ –3.0 J_V/MeV, and the imaginary potentials increase from low values of $J_W \approx 20$ at E = 0 MeV, at a rate of ≈ +3.0 J_W/MeV. The parameters of **Table V-A-1(A)** are strictly valid only for energies below ≈ 15 – 20 MeV. At higher energies volume absorption may become a contributing factor, and the imaginary strengths cannot continue to indefinitely increase with energy. Furthermore, these potentials do not consider dispersion effects, as discussed in **Sec. IV-C.**

The above potential strengths and the corresponding geometric parameters can be averaged to obtain "regional" values. The results are summarized in **Table V-A-1(B)**. With the appropriate β_2 and β_4 values, the "regional" potential of **Table V-A-1(B)** gives a remarkably good description of the tantalum experimental total cross sections, as illustrated in **Fig. V-A-1**. The results are essentially identical to those of the ROTM of **Table IV-B-1** and as illustrated in **Fig. IV-B-1**. Similar good agreement is found with other measured neutron total cross sections in this collective region. The differential scattering cross sections of tantalum calculated with the "regional" potential are very similar to those obtained with the ROTM, as is evident from comparing **Figs. IV-B-2** and **Fig. V-A-2.** Similar agreement was obtained for the other collective nuclei of **Table V-A-1(A)** using the "regional" potential of **Table V-A-1(B)**. This "regional" potential should be very suitable for the provision of data for basic and applied purposes up to incident energies of at least 20 MeV. Such applications would encompass a major portion of the fission product nuclei.

The real radius of the "regional" potential of **Table V-A-1(B)** is reasonably consistent with global mass-dependences, such as given by

$$r_V = 1.1685 + 0.37225/A^{1/3} \quad \textbf{Eq. V-A-1}$$

deduced from the systematic behavior of real radii in interpretations over a wide mass region (**Smi98**, Smith, A., 1998). The difference between the tantalum real radius of the "regional" potential and the systematic prediction is only 1.8%. This agreement is remarkable, given the well-known Vr real-potential parameter correlation. The imaginary radius of the "regional"

potential is somewhat larger than that of the real potential (by $\approx 0.5\%$), as is commonly encountered.

The strengths of the neutron optical potential are related to iso-spin through the expression

$$J_i = J_{0i}(1 - \xi_i \cdot \eta), \qquad \textbf{Eq. V-A-2}$$

where J_i and J_{0i} are real or imaginary potential strengths expressed in terms of volume-integrals-per-nucleon, η is the nuclear asymmetry (N-Z)/A, "i" may be V or W corresponding to real or imaginary potentials and ξ_i is a constant (**Lan62**). Neutron scattering studies generally lead to ξ_V values near unity (**FCR77**, Ferrer, Carlson and Rapaport, 1977; **HW72**, Holqvist and Wiedling, 1972; **Smi98**, Smith, 1998), which are nearly twice those deduced from nucleon-nucleon scattering and (p, n) studies. This discrepancy can be alleviated using the expression

$$J_V = (r_V)^3 \cdot K_{0V} (1 - \xi_V \cdot \eta), \qquad \textbf{Eq. V-A-3}$$

where K_{0V} is a constant and r_V has an appropriate mass dependence such as given by **Eq. V-A-1**, above (**Chi90**, Chiba et al., 1990). With the latter formulation, neutron measurements result in ξ_V values of ≈ 0.5, similar to those suggested by nucleon-nucleon scattering and (p, n) studies (**GMP**70, Greenlees, Makofske and Pyle, 1970; **GPT**68, Greenlees, Pyle and Tang, 1968; **BFG69**, Batty, Friedman and Greenlees, 1969). These iso-spin effects have negligible influence on the derivation of the present "regional" potential as the deformed targets under consideration span a mass range of approximately 155 to 186 where the asymmetry is on a plateau having values in the range 0.175 to 0.195. Such small variations in asymmetry lead to essentially negligible consequences in the deduction of a regional potential over this mass range.

The "regional" potential defines the effective mass, m^*, through the equation

$$m^*/m = 1 - dV^L/dE, \qquad \textbf{Eq. V-A-4}$$

where "m" is the nucleon mass and V^L the local real potential. This ratio, following from the above "regional" potential, is 0.702. Theoretical considerations of non-locality result in a ratio of

$$m^*/m = 0.64 + 0.36 \cdot [1 - ABS(E - E_F)/(2\hbar W_0)]^2, \qquad \textbf{Eq. V-A-5}$$

where E_F is the Fermi Energy and $\hbar W_0 = 41/A^{1/3}$ (**BDS79**, Brown, DeHesa and Speth, 1979; **MN81**, Mahaux and Ngo, 1981). Well away from E_F, **Eq. V-A-5** leads to the ratio $m^*/m = 0.68$. The latter value is only $\approx 3\%$ from that resulting from the above "regional" potential. The "regional" potential implies a zero end-point of 157.98 MeV, compared with 167.68 MeV deduced from the general potential of Bauer et al. (**Bau+82**, Bauer et al., 1982). The latter resulted from a global analysis of spherical and "near spherical" proton potentials. Thus, aspects of the present collective "regional" potential are remarkably consistent with those resulting from considerations of global spherical and near spherical potentials. This is not true of the above

SOM and dispersive interpretations in this collective region, as the resulting energy dependencies of the respective real potentials are quite different, and even erratic. This is probably due to the fact that the SOM is essentially a parameterization, which is not physically realistic in this collective region. In the dispersive applications the energy dependence of the real potential can vary a great deal depending upon the details of the formulation so deviations from the predictions of **Eq. V-A-4** are not surprising. The energy dependence of the SOM real potential is not entirely due to non-locality but is also influenced by dispersive contributions. This dispersive effect in the interpretation of the non-locality of the nuclear force has apparently not been well considered in the literature.

V-B. Comparisons with the ENDF/B-VI Evaluated File

The elemental tantalum (i.e.^{181}Ta) ENDF/B-VI file (MAT-7328) does not benefit from any recent experimental results or from the use of contemporary calculational models. The evaluated neutron total cross sections are compared with the present experimental database in Panel A of **Fig. V-B-1**. The evaluated and measured total cross sections are in relatively good agreement from several MeV to 20 MeV. However, the total cross-section evaluation is much lower than the measured values at lower energies. There is one set of experimental data that has very small magnitudes at lower energies, as noted in **Appendix A**. That data is a part of a group of total cross-section measurements at a single institution, the magnitudes of which are generally considerably smaller than those of a number of other published results. The problem is well known, and for that reason those results were not included in constructing the present average total cross sections. The lower values of the ENDF/B-VI total cross sections below several MeV are not supported by any of the models of the present interpretations, nor by low-energy trends of total cross sections in this mass region. Apparently, ENDF/B-VI placed principal reliance on one particular set of doubtful low-energy-total-cross-section data. Since the files are internally consistent, these significantly lower total cross sections will impact on the partial cross sections in an energy region important to many applications (e.g., fast fission reactors).

The ENDF/B-VI elastic scattering cross sections are compared with those predicted by the ROTM of **Sec. IV-B** in Panel B of **Fig. V-B-1**. Above ≈ 5.0 MeV the two elastic cross sections are in reasonably good agreement. Below 1.0 MeV the differences become very large with decreasing energy, amounting to 25% or more near 1.0 MeV. This is doubtless a reflection of the total cross section differences noted above. Illustrative differential elastic-scattering distributions predicted by the ROTM of **Sec. IV-B** are compared with those of ENDF/B-VI at representative energies of 1.0, 4.0, 10.0 and 15.0 MeV in **Fig. V-B-2**. These differential results are very different below ≈ 5.0 MeV, but are qualitatively similar at higher energies. It is reasonable to expect large differences between measured and ENDF/B-VI values in other reaction channels at the lower energies where the evaluated total cross sections appear to be in considerable error.

VI. CONCLUDING REMARKS

The energy-averaged neutron total cross sections of elemental tantalum are reasonably known from several MeV to several-hundreds of MeV. This is important as total cross sections are an envelope that models and evaluations must conform to. Furthermore, neutron processes are unique in that they allow the direct determination of nuclear total cross sections by simple transmission measurements. This advantage is not true of charged-particle processes, which are inhibited by coulomb effects at lower energies. Below several MeV there are large discrepancies between measured neutron total cross sections of tantalum that contribute to evaluation and model uncertainties. Therefore:- **Recommendation 1** – The neutron total cross sections of tantalum should be carefully measured from several-tens of keV to several MeV at few-keV intervals. Attention must be given to self-shielding, in-scattering, sample-size, dead time and other experimental perturbations. Such measurements are not difficult but must be done carefully if an accuracy goal of ≈ 1 % is to be realized.

The "elastic"-scattering cross sections of elemental tantalum are now reasonably known from $\approx 0.3 - 1.5$ MeV, and from $\approx 4.5 - 15.2$ MeV. In between the available information is sparse and dubious. There is nothing above ≈ 15.2 MeV. Therefore:- **Recommendation 2** – Careful differential "elastic"-scattering measurements at a number of energies between 1.5 and 4.5 MeV and above 16.0 MeV should be made. These will be difficult and will not resolve the elastic component from the first (or few) inelastic contributions. The angle and energy resolutions must be as good as practicable, and results must be fully corrected for experimental perturbations. Accuracy goals should be $\approx 2 - 3$% in regions of appreciable cross-section magnitudes, and twenty or more angular differential measurements should be made at each incident energy.

Very little is known of the neutron inelastic scattering from elemental tantalum. At least three collective rotational bands contribute to such processes, and the limited available results below incident energies of ≈ 1.5 MeV suggest that the excited structure of tantalum is not well known at relatively low energies. Experimental inelastic neutron-scattering studies have the unique potential of the low-energy neutron probe. Therefore:- **Recommendation 3** -- Neutron-detection inelastic scattering and (n; n',γ) cross sections should be measured in complimentary detail over incident-neutron energies of < several MeV. Advantage should be taken of coincident techniques. These are not easy measurements but are now promising with recent advances in high-resolution γ-ray detection. Attention must be given to experimental energy resolutions, corrections and calibration factors. These results would be useful for both basic and applied purposes. In particular, they offer the potential for resolving structure uncertainties and of providing new insight into the collective reaction mechanisms.

Over the last few years the capability of models to handle collective vibrational and rotational nuclei has grossly improved. However, the models demand knowledge of the underlying physical mechanisms which, in tantalum, are far from well known. What is done in the present work is a first approximation. Furthermore, most available calculational vehicles will not fit experimental data, concurrently dealing with neutron differential-scattering and total cross sections, nor with several isotopes if that is the case (it is not so for tantalum). Also other

reaction channels should be considered. **Recommendation 4** -- Continued attention should be given to enhancing and extending modeling capability. This is particularly promising due to the rapid advances in computational systems and capability.

Dispersive effects are a concern in the context of both basic and applied understanding. The exact formulation of such contributions is a matter of theoretical debate, but dispersive effects will affect such matters as potential energy dependencies and thus, for example, consideration of the non-locality of the nuclear forces.

Despite the above shortfalls, the present and recent work at Argonne and Los Almos have resulted in a "regional" collective model that provides a remarkably satisfactory description of the neutron interaction with nuclei in the collective region of $A \approx 150 - 190$. As more information becomes available, this "regional" model can be refined. It encompasses many of the heavy fission-product nuclei of applied interest. Even at this point, it suggests some major changes in the current ENDF/B-VI evaluation of elemental tantalum.

ACKNOWLEDGEMENTS

The author would like to thank Drs. J. Raynal, P. Young and F. Kondev for their continued technical advice and comment. The author is also indebted to the National Nuclear Data Center for the provision of essential nuclear-neutron data, and to Mr. John Bolling and his associates for constructing the computing facilities used in much of this work.

REFERENCES

(Bau+82) Bauer, M. et al., 1982, J. Phys. **G8** 525.
(BDS79) Brown, G., Dehesa, J. and Speth, J., 1979, Nucl. Phys. **A330** 290.
(BFG69) Batty, C., Friedman, E. and Greenlees, G., 1969, Nucl. Phys. **A127** 368.
(Bud+82) Budtz-Jorgensen, C., el al., 1982, Z. Phys. **A360**, 265.
(Chi+90) Chiba, S., et al., 1990, Phys. Rev. **C42** 2487.
(Chi+92) Chiba, S., et al., 1992, Phys. Rev. **C45** 1260.
(CL55) Cranberg, L. and Levin, J., 1955, **Proc. Conf. on Peaceful Uses of Atomic Energy**, Geneva, United National Press.
(CSL83) Conde, H., Smith, A. and Lorenz, A., 1983, IAEA Tech. Report **IAEA-227**.
(Dra+98) Dracoulis, G., et al., 1998, Phys. Rev. **C58** 1837.
(Dro87) Drosg, M., 1987, IAEA Report **IAEA-TECDOC-410**.
ENDF/B-VI) Evaluated Nucl. Data File-B, Version-VI, available from the National Nuclear Data Center, Brookhaven Natl. Lab.
(FCR77) Ferrer, J., Carlson, J. and Rapport, J., 1977, Nucl. Phys. **A275** 325.
(Fes58) Feshbach, H., 1958, Ann. Rev. Nucl. Sci. **8** 49.
(FPW54) Feshbach, H., Porter, C. and Weisskopf, V., 1954, Phys. Rev. **96** 448.
(GC65) Gilbert, A. and Cameron, A., 1965, Can. J. Phys. **43** 1446.
(GMP70) Greenlees, G., Makofske, W. and Pyle, G., 1970, Phys. Rev. **C1** 1145.

(GPT68) Greenlees, G., Pyle, G. and Tang, Y., 1968, Phys. Rev. **171** 1115; also 1970, Phys. Rev. **C1** 1145.

(Hod63) Hodgson, P., 1963, **The Optical Model of Elastic Scattering,** Clarendon, Oxford.

(HW72) Holmqvist, B. and Wiedling, T., 1972, Nucl. Phys. A188 24.

(JLM77) Jeukenne, J., Lejeune, A. and Mahaux C., 1977, Phys. Rev. **C16**, 80.

(KD03) Koenig, A. and Delaroche, J., 2003, Nucl. Phys. **713**, 231.

(Kon04) Kondev, F., 2004, private communication.

(Lan61) Lane, R., et al.,1961, Ann. Phys. **12** 135.

(Lan62) Lane, A., 1962, Nucl. Phys. **35** 676; also 1962, Phys. Rev. Lett. **8** 171.

(LGS87) Lawson, R., Guenther, P. and Smith, A., 1987, Phys. Rev. **C36** 1287.

(Lip66) Lipperheide, R., 1966, Nucl. Phys. **89** 97.

(LS99) Lawson, R. and Smith, A., 1999, Argonne Natl. Lab. Report **ANL/NDM-145**.

(LS01) Lawson, R. and Smith, A., 2001, Argonne Natl. Lab. Report **ANL/NDM-152**.

(MN59) Mottelson, B. and Nilsson, S., 1959, Kgl. Danske Videnskab Selskab. Mat. Fys, Skrifter **1** 8.

(MN81) Mahaux, C. and Ngo, N., 1981, Phys. Lett. **B100** 285.

(Mob77) Mobley, R., 1977, USAEC Report **AT-(40-1)**.

(Mol80) Moldauer, P., 1980, Nucl. Phys. **A344** 185.

(Mug+81) Mughabghab, S. et al., 1981, **Neutron Cross Sections,** Academic, New York.

(NDS92) Nuclear Data Sheets, 1992, Firestone, R., Available from the National Nuclear Data Center, Brookhaven Natl. Lab.

(Pas67) Passatori, G., 1967, Nucl. Phys. **A95** 694.

(PB62) Perey, F. and Buck B., 1962, Nucl. Phys. **32** 353.

(Pre62) Preston, M., 1962, **The Physics of the Nucleus**, Addison-Wesley, Reading, MA.

(Ray94) Raynal, J., 1994, CEA Report **CEA-N-2772**, also private communication.

(Sat83) Satchler, G., 1983, **Direct Nuclear Reactions**, Addison-Wesley, Reading, Ma.

(SG92) Smith, A. and Guenther, P.,1992, Argonne Natl. Lab. Report **ANL/NDM-127**.

(SGS77) Smith, A., Guenther, P. and Sjoblum, R., 1977. Nucl. Instr. and Meth. **140** 397.

(SGW68) Smith, A., Guenther, P. and Whalen, J., 1968, Phys. Rev. **168** 1344.

(Smi+63) Smith, A., et al., 1963, Argonne Natl. Lab. Report **ANL-6723**.

(Smi+67) Smith, A., el al., 1967, Nucl. Instr. Meth. **50** 277,

(Smi91) Smith, A., 1991, Argonne Natl. Lab. Memorandum, unpublished.

(Smi98) Smith, A., 1998, J. Phys. **G24** 634.

(Smi00) Smith, A., 2000, Argonne Natl. Lab. Report **ANL/NDM-151**, also 2001. Ann Nucl. Energy **28** 1745.

(Smi01) Smith, A., 2001, Argonne Natl. Lab. Report **ANL/NDM-153**, also 2002, Ann. Nucl. Energy **28** 1241.

(Smi03) Smith, A., 2003, Argonne Natl. Lab. Report **ANL/NDM-155**, also 2004, J. Phys. **G30** 407.

(Smi04) Smith, A., 2004, Argonne Natl. Lab. Report **ANL/NDM-157**, also 2004, Ann Nucl. Energy **31** 1813.

(Smi05) Smith, A., 2005, to be published.

(Tam65) Tamura, T., 1965, Rev. Mod. Phys. **37** 679.
(Tul90) Tuli, J., 1990, Nuclear Wallet Cards, National Nuclear Data Center, Brookhaven Natl. Lab.
(WG85) Walter, R. and Guss, P., 1985, **Proc. Conf. on Nucl. Data for Basic and Applied Sci.**, Eds. Young, P. et al., **2** 272, Gordon and Breach, New York.
(Wol51) Wolfenstein, L., 1951, Phys. Rev. **82** 690.
(YA87) Young, P. and Arthur, E., 1987, Los Alamos Natl. Lab. Report **LA-10915-PR** 31.

APPENDICIES

Appendix A. Total Cross-Section Experimental Data Base

CINDA cites twenty one references to measurements of fast-neutron total cross sections of tantalum relevant to the present considerations. These works are referenced below. There are a few additional total-cross-section citations, which are; not pertinent to the present work (e.g. low-energy and/or resonance data), with obviously erroneous data, or are redundant citations. The relevant referenced work spans nearly half a century, with an average age of over forty years. The numerical values of these data sets were assembled from the data files of the National Nuclear Data Center (**NNDC**). Since the present work considers energy-averaged cross sections, the data of each set was averaged over 10 keV intervals below 0.1 MeV, over 0.1 MeV intervals from 0.1 to 0.5 MeV, over 0.2 MeV intervals from 0.5 to 5.0 MeV and over 0.25 MeV intervals at energies above 5.0 MeV. These averaging increments were chosen so as to portray the general energy-dependent behavior of the cross sections while remaining consistent with the experimental resolutions of the present measurements and with the model concepts used in the interpretations. All of the averaged data sets were then combined and ordered by energy to form a master total cross section data file. This master file was inspected for obviously erroneous values, which were culled, and then combined by again averaging over the above increments. The result is shown in **Fig. A-1 (A)**. The agreement between the individual averaged data sets is generally remarkably good from a few tens of keV to 600 MeV. **Figs. A-1(B)** and **A-1(C)** portray the same total cross- section results on expanded energy scales of 0 - 100 and 0 - 20 MeV, respectively. The curve in **Fig. A-1(C)** indicates the corresponding **ENDF/B-VI** total cross- section values. The agreement between measurements and evaluation is good except below several MeV where the **ENDF/B-VI** results fall considerably below the experimental averages. It is a region where the models described in the above text can give some guidance.

Total Cross Section References

(Boc+49) Bockelman, C., et al., 1949, Phys. Rev. **76** 277, #11881.
(Bra+58) Bratenahl, A., et al., 1958, Phys. Rev. **110** 927, #11155.
(CB67) Carlson, A. and Barschall, H., 1967, Phys. Rev.**158** 1142, #11497.
(CINDA) Computerized Index of Neutron Data, available from the NNDC.
(Con58) Conner, J., 1958, Phys. Rev. **109** 1268, #11320.
(Coo+52) Coon, J., et al., 1952, Phys. Rev. **88** 562, #11056.

(Div68) Divadeenam, T., 1968, **DA/B-28** 3834, #10523.
(ENDF/B-VI) Evaluated Nuclear Data File/B-VI, available from the NNDC.
(Fin+93) Finlay, R., et al., 1993, Phys. Rev. **C47** 234, #13569.
(FG71) Foster, D. and Glasgow, D., 1971, Phys. Rev. **C3** 576, #10047.
(Fra+88) Franz, J, et al., 1988, Nucl. Phys. **A490** 667, #22117.
(Hau58) Haugness, T., 1958, **DA/B-28** 3835, #11733.
(HL50) Hildebrand, R. and Leith, C., 1950, Phys. Rev. **80** 842, #11039.
(Man70) Manero, F., 1970, ARS **66** 27, #20171.
(Mar+67) Martin, R., et al., 1967, BAPS **12** 106, #12159.
(ND54) Nereson, N. and Darden, S., 1954, Phys. Rev. **94** 1674, #11308.
(NNDC) National Nuclear Data Center, Brookhaven Natl. Lab., Upton NY.
(Pet+60) Peterson, J., et al., 1960, Phys. Rev. **120** 521, #11108.
(Poe+81) Poenitz, W., et al., 1981, Nucl. Sci. Eng. **78** 333, #10935.
(PW83) Poenitz, W. and Whalen, J., 1983, **ANL/NDM-80**. #12853.
(Rag53) Ragent, B., 1953, **UCRL-2337**, #11338.
(Smi+68) Smith, A., et al., 1968, Phys. Rev. **168** 1344, #10631.
(Tab+64) Tabony, R., et al., 1964, Phys. Lett. **13** 70, #11936.
(WB55) Walt, M. and Beyster, R., 1955, Phys. Rev. **98** 677, #11215.

'#' denotes the relevant EXFOR number.

Appendix B. Prior Elastic Scattering Data Base

Experimental differential fast-neutron "elastic"-scattering data for tantalum relevant to the present considerations is cited in twenty two **CINDA** references as follows:-

Differential fast-neutron elastic-scattering references:-

(Bec+66) Becker, R., et al., 1966, Nucl. Phys. **89** 154, 3.2 MeV distribution, #11511.
(Ben+73) Benenson, R., et al., 1973, Nucl. Phys. **A212** 147, 14.8 MeV distribution, #11037.
(Bey+56) Beyster, R., et al., 1956, Phys. Rev. **104** 1319, 2.5 and 7.5 MeV distributions, #11495.
(Buc+66) Buccino, S., et al., 1966, Z. Phys. **196** 103, 5.0 MeV distribution, #11877.
(CC72) Cox, S. and Cox, E., 1972, Argonne Report **ANL-7935**, 0.9 MeV distribution, #10332.
(CINDA) Computerized Index to Neutron Data, available from the NNDC.
(CJ60) Cross, W. and Jarvis, R., 1960, Nucl. Phys. **15** 155, 14.6 MeV distribution, #11465.
(Ell56) Elliot, J., 1956, Phys. Rev. **101** 684, 14.1 MeV distributionm #11568.
(Fer+77) Ferrer, J., et al., 1977, Nucl. Phys. **A275** 325, 11.1 MeV distribution, #10633.
(GT63) Gilboy, W. and Towle, J., 1963, Nucl. Phys. **42** 86, 0.98 MeV distribution, #21110.
(Han+85) Hansen, L., et al., 1985, Phys. Rev. **C31** 111, 14 MeV distribution, #12935.
(Hol+69) Holmqvist B., et al., 1969, Report **AE-366**. Seven distributions between 2.5 and

8.0 MeV, #20019.
(Hud+62) Hudson, C., et al., 1962, Phys. Rev. **128** 1271, 15.2 MeV distribution, #12180.
(NNDC) National Nuclear Data Center, Brookhaven Natl. Lab.
(Rem56) Remund, A., 1956, Helv. Phys. Acta **29** 545, 3.3 MeV distribution, #21242.
(Rod+61) Rodgers, W., et al., 1961, BAPS **6**, 0.7 and 0.9 MeV distributions, #11269.
(RS57) Rosen, L. and Stewart, L., 1957, Phys. Rev. **107** 824, 14.0 MeV distribution, #11223.
(Sch+89) Schreder, G., et al., 1989, Phys. Rev. **C39** 1768, 7.7 MeV distribution, #22171.
(Smi+63) Smith, A., et al., 1963, Report **ANL-6723**, 24 distributions between 0.3 and 1.5 MeV, #12175.
(SGW68) Smith, A., Guenther, P. and Whalen, J., 1968, Phys. Rev. **168** 1344, 98 distributions between 0.3 and 1.5 MeV, # 10631.
(Tak+89) Takahashi, A., et al., 1989, Report **INDC(JAP)-118/L**, 14.1 MeV distribution, #22136.
(WB54) Walt, M. and Barschall, H., 1954, Phys Rev. **93** 1062, 1.0 MeV distribution, #11637.
(WB55) Walt, M. and Beyster, R., 1955, Phys. Rev. **98** 677, 4.1 MeV distribution, #11215.
(Yos+65) Yoshimura, A., et al., 1965, Report **EANDC(J)-1** 24, 14.1 MeV distribution, #20266.
'#' denotes relevant EXFOR number.

The average age of these references is nearly 40 years, and all are at least 15 years old. The vast majority of the experimental-data is from the early and low-energy work of the author and his associates (**Smi+63**, Smith et al., 1963; **SGW68**, Smith, Guenther and Whalen, 1968) nearly forty years ago, as discussed in the body of this report.

Appendix C. Prior Inelastic-Scattering Data Base

Experimental fast-neutron inelastic-scattering data relevant to the present considerations is cited in only four **CINDA** references, as follows:-

Differential fast-neutron inelastic scattering references:-

(CINDA) Computerized Index of Neutron Data, available from the NNDC.
(GT63) Gilboy, W. and Towle, J., 1963, Nucl. Phys. **42** 86, #21220.
(GW56) Guernsey, J. and Wattenberg, A., 1956, Phys. Rev. **101** 1516, #11691.
(NNDC) National Nuclear Data Center, Brookhaven Natl. Lab.
(SAF54) Scherrer, V., Allison, B. and Faust, 1954, W., Phys. Rev. **96** 386, #11673.
(SGW68) Smith, A., Guenther, P. and Whalen, J., 1968. Phys. Rev. **168** 1344, #10631.
"#" denotes relevant EXFOR number.

Of these only the early work by the author and associates (**SGW68,** Smith, Guenther and

Whalen. 1968) makes a significant contributions to the present considerations. Those results are incorporated in the present work as discussed in **Sec. IV-B**. References (**SAF54**, Scherrer, Allison and Faust, 1954) and (**GW56**, Guernsey and Wattenberg, 1956) deal with early (n;n',γ) measurements using NaI(Tl) detectors and do not directly result in inelastic-neutron-scattering cross sections. The remaining citation, (**GT63**, Gilboy and Towle, 1963) is relative to a single unresolved elastic+inelastic scattering measurement at an incident energy of 0.98 MeV. This is a very weak neutron inelastic-scattering database for either basic or applied considerations.

TABLES

Table IV-A-1 SOM parameters obtained using four-parameter fitting and the real and imaginary diffusenesses of gadolinium (**Smi04**, Smith, 2004). Potential depths are in MeV, potential strengths in volume-integrals-per-nucleon (J_i, in MeV·fm^3), and geometric parameters in fms.

Real Potential

Strength

$V = 42.491 - 0.006962 \cdot E$

$J_V = 378.87 - 0.06207 \cdot E$

Reduced Radius

$r_v = 1.2526$

Diffuseness

$a_v = 0.6501$ (fixed)

Imaginary Potential

Strength

$W = 14.496 + 1.3463 \cdot E$

$J_W = 63.78 + 5.9224 \cdot E$

Reduced Radius

$r_w = 1.4108$

Diffuseness

$a_w = 0.2480$ (fixed)

Spin-Orbit Potential (**WG85**, Walter and Guss, 1985)

Strength

$V_{so} = 6.154 - 0.015 \cdot E$

Reduced Radius

$r_{so} = 1.103$

Diffuseness

$a_{so} = 0.560$

Table IV-A-2 SOM parameters obtained using four-parameter fitting with the real and imaginary diffusenesses of rhenium (**Smi03**, Smith, 2003). The nomenclature is identical to that of **Table IV-A-1**.

Real Potential

Strength

$V = 40.280 + 0.49943 \cdot E$

$J_V = 375.73 + 4.6590 \cdot E$

Reduced Radius

$r_V = 1.2715$

Diffuseness

$a_V = 0.6607$ (fixed)

Imaginary Potential

Strength

$W = 21.000 - 3.1558 \cdot E \quad (E < 5 \text{ MeV})$

$J_W = 103.88 - 8.6411 \cdot E - 1.0428 \cdot E^2$

$W = 2.5407 + 0.53508 \cdot E \quad (E > 5 \text{ MeV})$

$J_W = 13.008 + 3.3234 \cdot E + 0.19807 \cdot E^2$

Reduced Radius

$r_W = 1.2747$

Diffuseness

$a_W = 0.3391 + 0.02293 \cdot E$ (fixed)

Spin-Orbit Potential, same as for **Table IV-A-1**.

Table IV-B-1. ROTM parameters. Potential depths are in MeV, strengths (J_i, in MeV/fm^3) and geometry's in fermis. Real and imaginary potential geometries are fixed to the "regional" values of Smith (**Smi04**, Smith, 2004).

Real Potential

Strength

$V = 46.942 - 0.2621 \cdot E$

$J_V = 441.08 - 2.4627 \cdot E$

Radius

$r_V = 1.2568$ (fixed, see text)

Diffuseness

$a_V = 0.6292$ (fixed, see text)

Imaginary Potential

Strength

$W = 3.1230 + 0.1039 \cdot E + 0.02280 \cdot E^2$

$J_W = 21.61 + 0.7189 \cdot E + 0.1578 \cdot E^2$

$W = 16.630 + 3.1660 \cdot E$ (linear approximation)

Radius

$r_W = 1.2629$ (fixed, see text)

Diffuseness

$a_W = 0.4785$ (fixed, see text)

Spin-orbit Potential (**WG85**, Walter and Guss, 1985)

Strength

$V_{SO} = 6.154 - 0.015 \cdot E$

Radius

$r_{SO} = 1.1030$

Diffuseness

$a_{SO} = 0.5600$

Deformation Parameters (**Kon04**, Kondev, 2004)

$\beta_2 = 0.269$

$\beta_4 = -0.090$

Table IV-C-1. Dispersive SOM parameters deduced as discussed in the text. Potential depths are in MeV and geometric parameters in fermis. The geometry is fixed to the values of rhenium (**Smi03**, Smith, 2003).

Real Potential

Depth

$V = 40.303 + 0.63726 \cdot E$

Reduced radius

$r_V = 1.2196$ (fixed)

Diffuseness

$a_V = 0.6607$ (fixed)

Imaginary Potential

Depth

$W = 3.3572 + 0.3329 \cdot E$ (above 7 MeV)

$W = 19.0 - 1.7581 \cdot E$ (below 7 MeV)

Reduced radius

$r_W = 1.3384$ (fixed)

Diffuseness

$a_W = 0.3391 + 0.02293 \cdot E$ (fixed)

Spin-Orbit Potential (as given in **Table IV-A-1**)

Table IV-C-2. Dispersive ROTM parameters deduced as discussed in the text. The geometries are fixed to the "regional" potential of Smith (**Smi04**, Smith, 2004). The nomenclature is the same as that of **Table IV-C-1**.

Real Potential

Depth

$$V = 46.068 - 0.03373 \cdot E$$

Radius

$$r_V = 1.2568 \quad \text{(fixed)}$$

Diffuseness

$$a_V = 0.6292 \quad \text{(fixed)}$$

Imaginary Potential

Depth

$$W = 1.9454 + 0.49428 \cdot E$$

Radius

$$r_W = 1.2629 \quad \text{(fixed)}$$

Diffuseness

$$a_W = 0.4785 \quad \text{(fixed)}$$

Spin-Orbit Potential same as in **Table IV-A-1**.

Deformation Parameters same as in **Table IV-B-1**.

Table V-A-1(A). Comparative potential strengths in volume-integrals-per nucleon (MeV/Fm^3).

Target	Z	A	η	β_2	J_i	ref.
Eu	63	152.0	0.171	0.160	J_V=455.95-3.147·E	**YA87**
					J_W= 20.0+3.846·E	
Gd	64	157.3	0.186	0.300	J_V=434.44-0.796·E	**Smi04**
					J_W=25.9+2.453·E	
Gd	64	157.3	0.186	0.300	J_V=434.81-2.059·E	**YA87**
					J_W=17.4+2.708·E	
Ho	67	164.9	0.188	0.300	J_V=444.39-3.558·E	**Smi00**
					J_W=22.4+2.151·E	
Ho	67	164.9	0.188	0.300	J_V=449.97-3.125·E	**YA87**
					J_W=25.5+2.363·E	
Hf	72	178.5	0.191	0.287	J_V=457.15-2.593·E	**Smi01**
					J_W=19.5+2.419·E	
Ta	73	181.0	0.193	0.269	J_V=441.08-2.463·E	**This work.**
					J_W=16.6+3.166·E	
Re	75	186.2	0.194	0.220	J_V=428.94-3.189·E	**Smi03**
					J_W=18.3+2.258·E	
Re	75	186.2	0.194	0.220	J_V=432.71-2.780·E	**MY87**
					J_W=16.5+4.931·E	

Table V-A-1(B). Parameters of the "regional" potential described in the text.

Real Potential

J_V = 442.6 – 2.8017·E (MeV/fm^3)

V = 47.1038 – 0.29817·E (MeV)

r_V = 1.2568 (fm)

a_V = 0.6292 (fm)

Surface-Imaginary Potential

J_W = 20.233 + 2.922·E (MeV/fm^3)

W = 2.9236 + 0.42222·E (MeV)

r_W = 1.2629 (fm)

a_W = 0.4785 (fm)

Spin-Orbit Potential

V_{so} = 6.14 – 0.015·E (MeV)

r_{so} = 1.103 (fm)

a_{so} = 0.560 (fm)

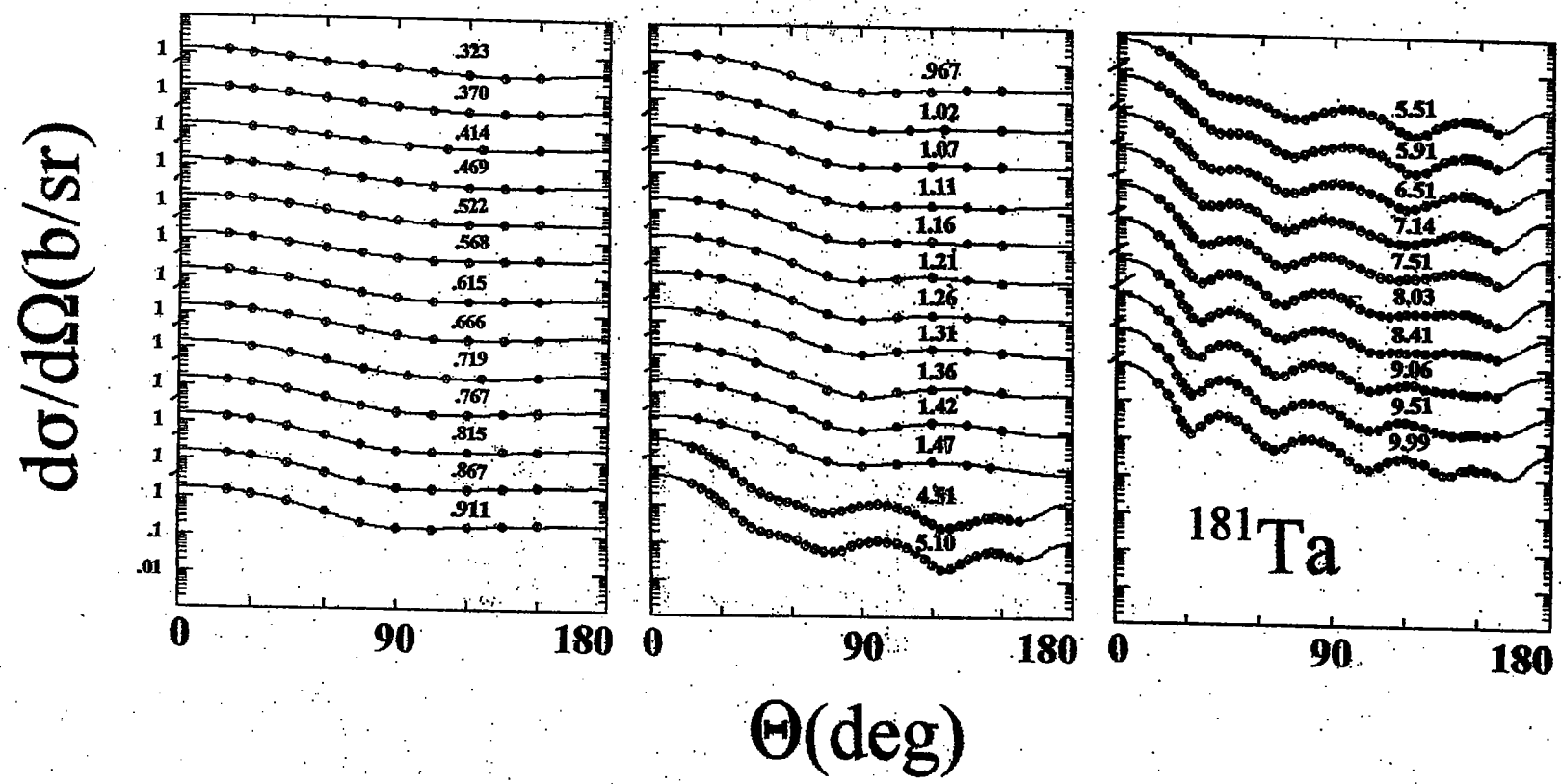

Fig. III-1. Averaged differential "elastic" distributions of neutrons scattered from elemental tantalum. The present experimental values are indicated by symbols, and the results of fitting the measurements with legendre-polynomial expansions by curves. Average incident-neutron energies are numerically noted in MeV. The figure contains both Part-A and Part-B results, as defined in the text. Throughout this report, angular distributions are presented in the laboratory coordinate system.

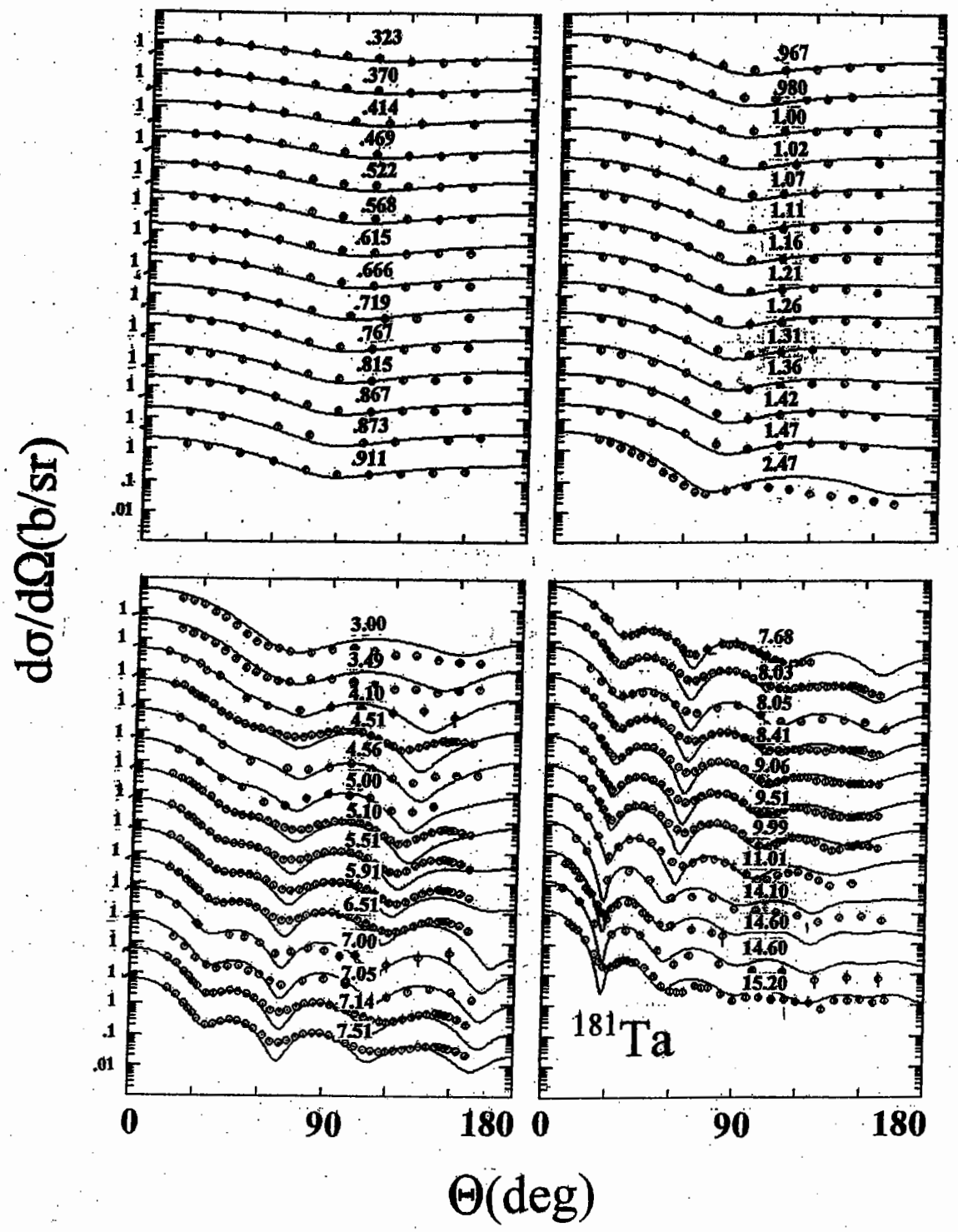

Fig. IV-A-1. Comparisons of measured (symbols) and SOM-calculated (curves) differential "elastic"-scattering cross-sections of tantalum. The calculations used the parameters of **Table IV-A-1**, as discussed in the text. Incident neutron energies are numerically indicated in MeV. These calculations involve 4-parameter fitting with the real and imaginary diffusenesses of Gd. All values are in the laboratory coordinate system.

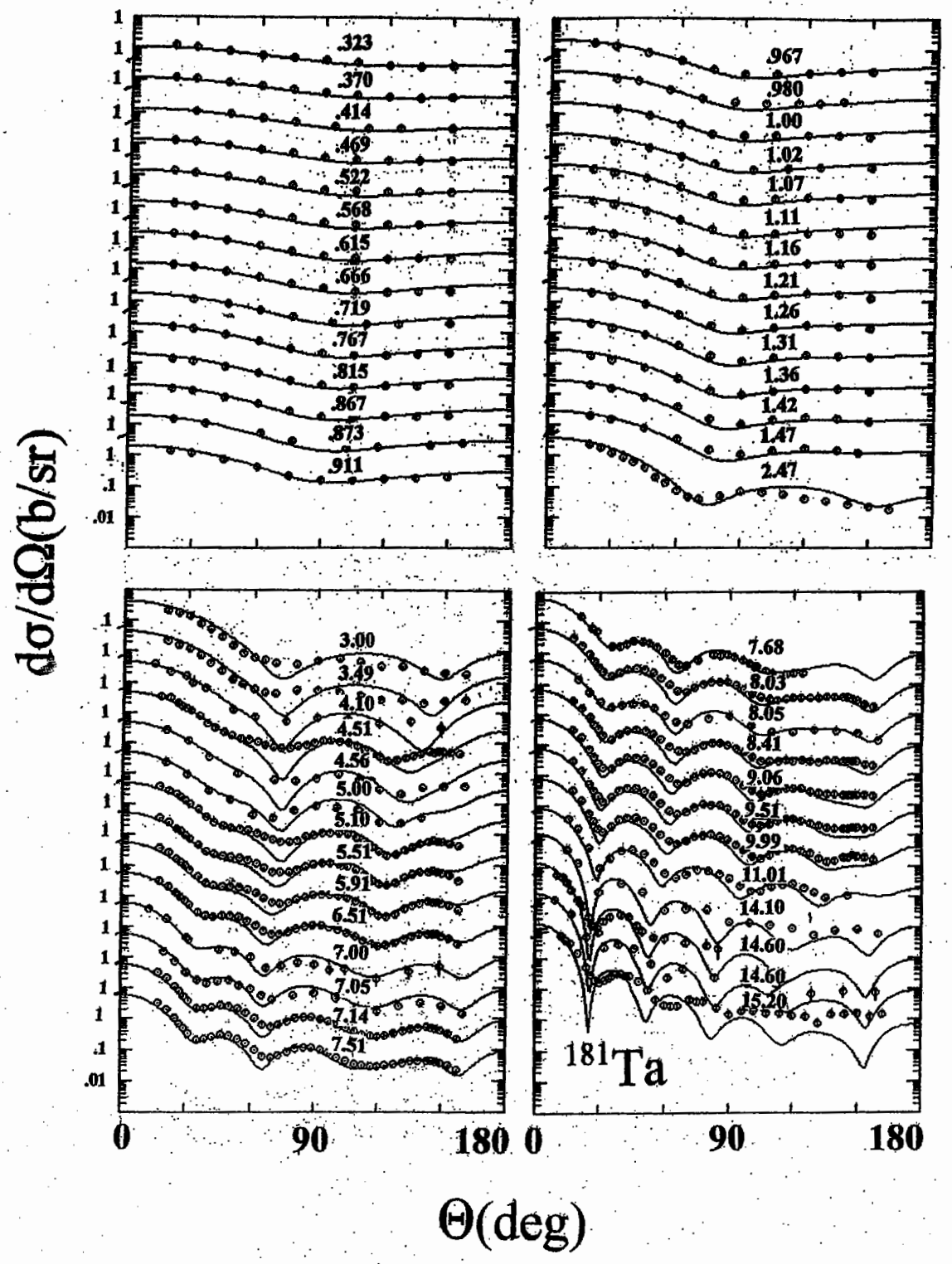

Fig, IV-A-2. Comparisons of measured (symbols) and calculated (curves) differential "elastic" scattering cross sections of tantalum. The calculations used the parameters of **Table IV-A-2** with Re real and imaginary diffusenesses, as discussed in the text. The nomenclature is identical to that of **Fig. IV-A-1.**

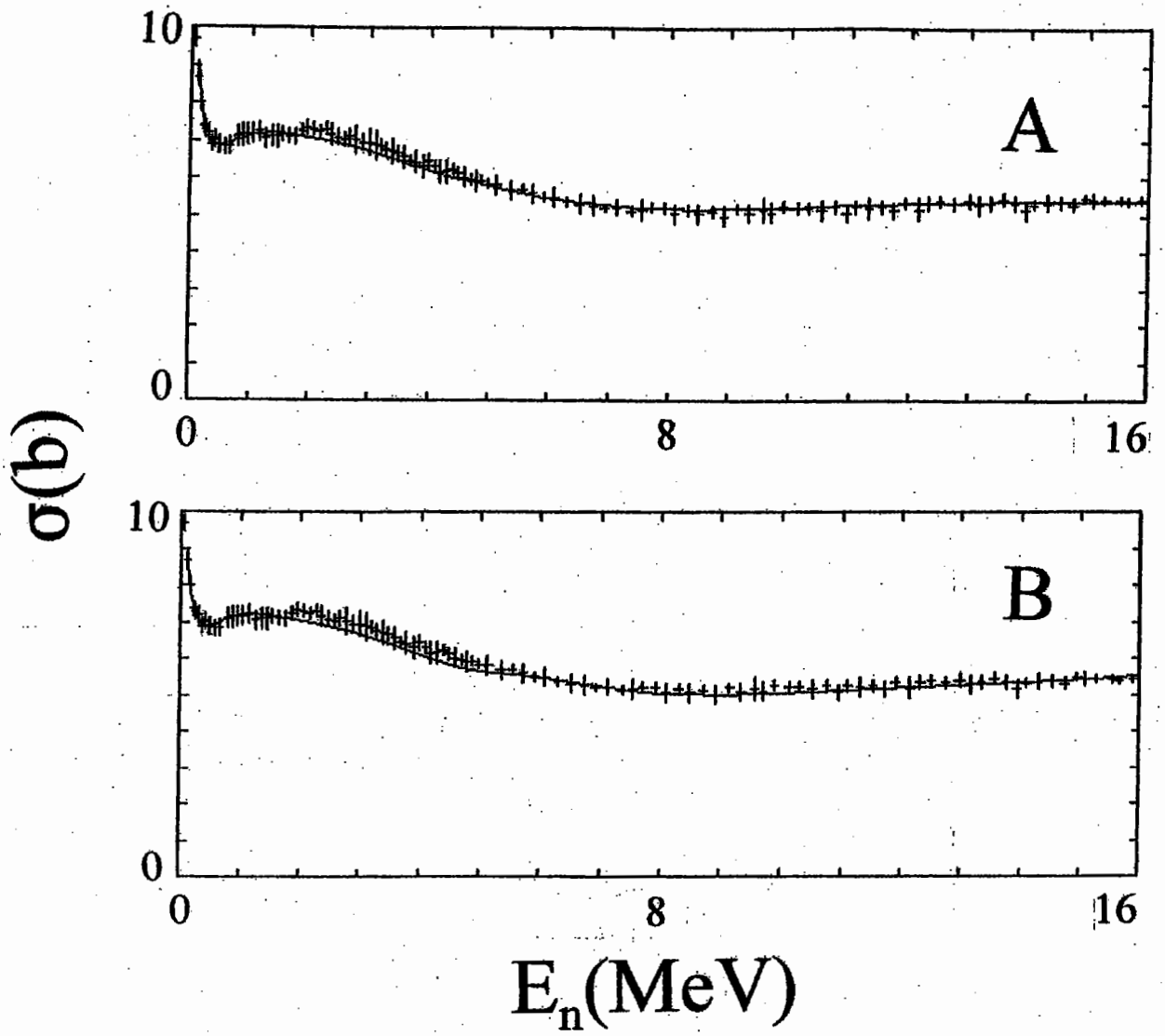

Fig. IV-A-3. Comparisons of measured and calculated neutron total cross sections of tantalum. Symbols indicate the energy-averaged experimental results as defined in **Appendix A**. Curves denote the results of SOM calculations. The calculations shown in Panel A were obtained with the potential of **Table IV-A-1**, and those of Panel B with the potential of **Table IV-A-2**.

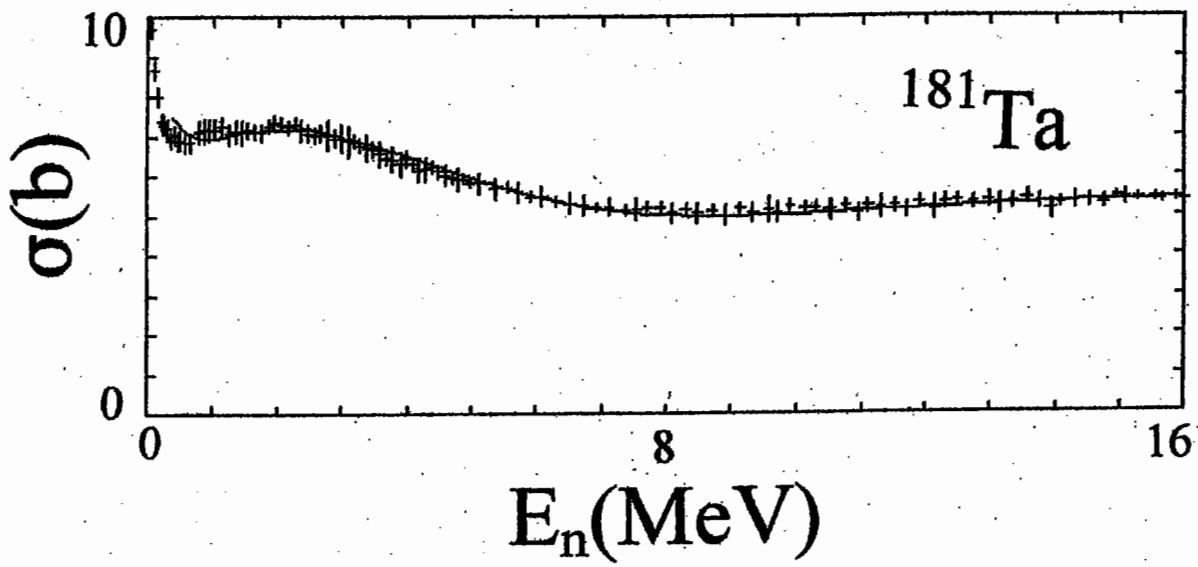

Fig. IV-B-1. Comparison of measured (symbols) and calculated (curve) neutron total cross sections of Ta. The calculations used the ROTM of **Table IV-B-1**.

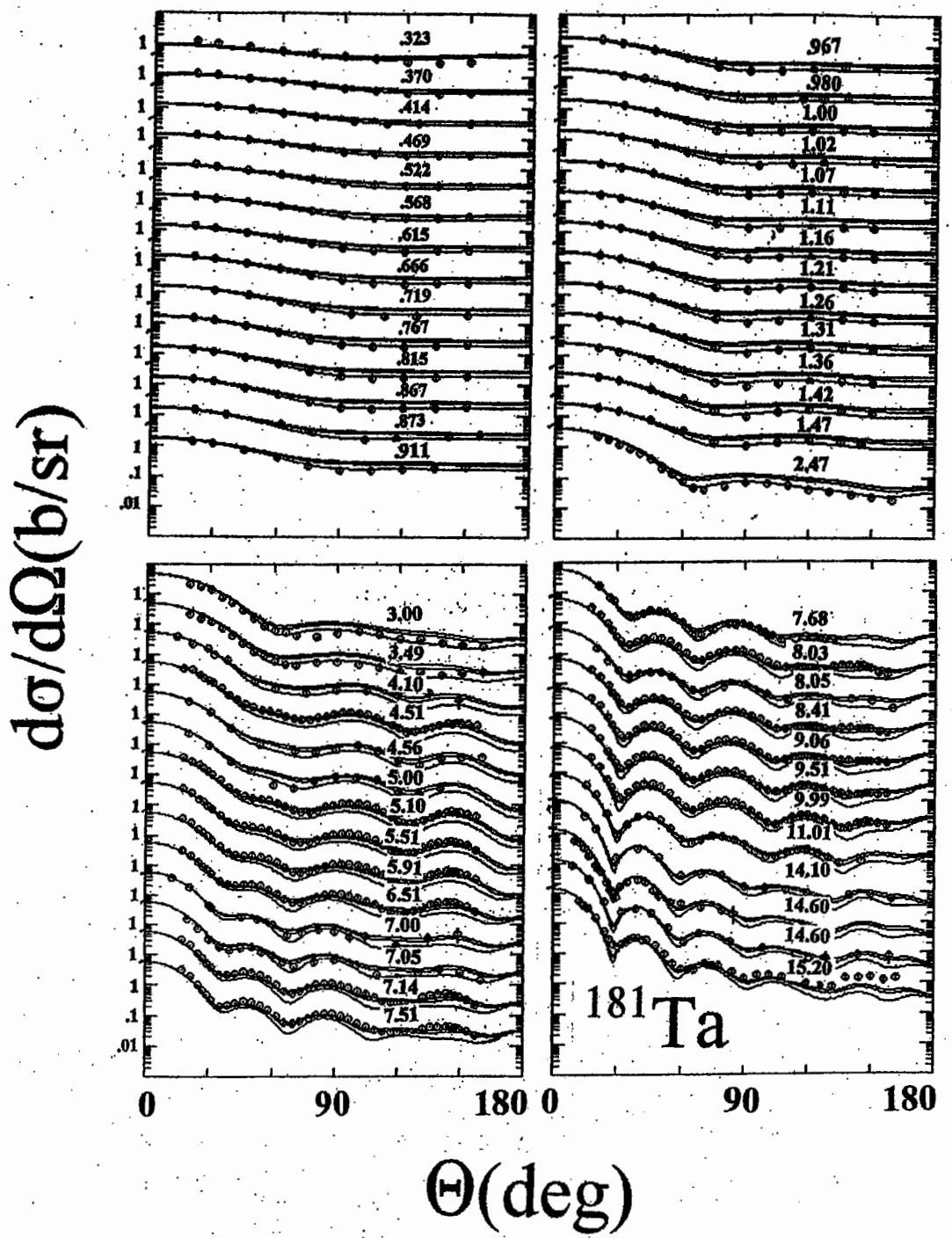

Fig. IV-B-2. Comparison of measured (symbols) and calculated (curves) differential "elastic"-scattering cross sections of tantalum. The calculations were made using the ROTM potential of **Table IV-B-1.** The three calculated distributions at each energy reflect alternate choices of experimental resolutions, as described in the text. Otherwise, the nomenclature of this figure is the same as that of **Fig. IV-A-1**.

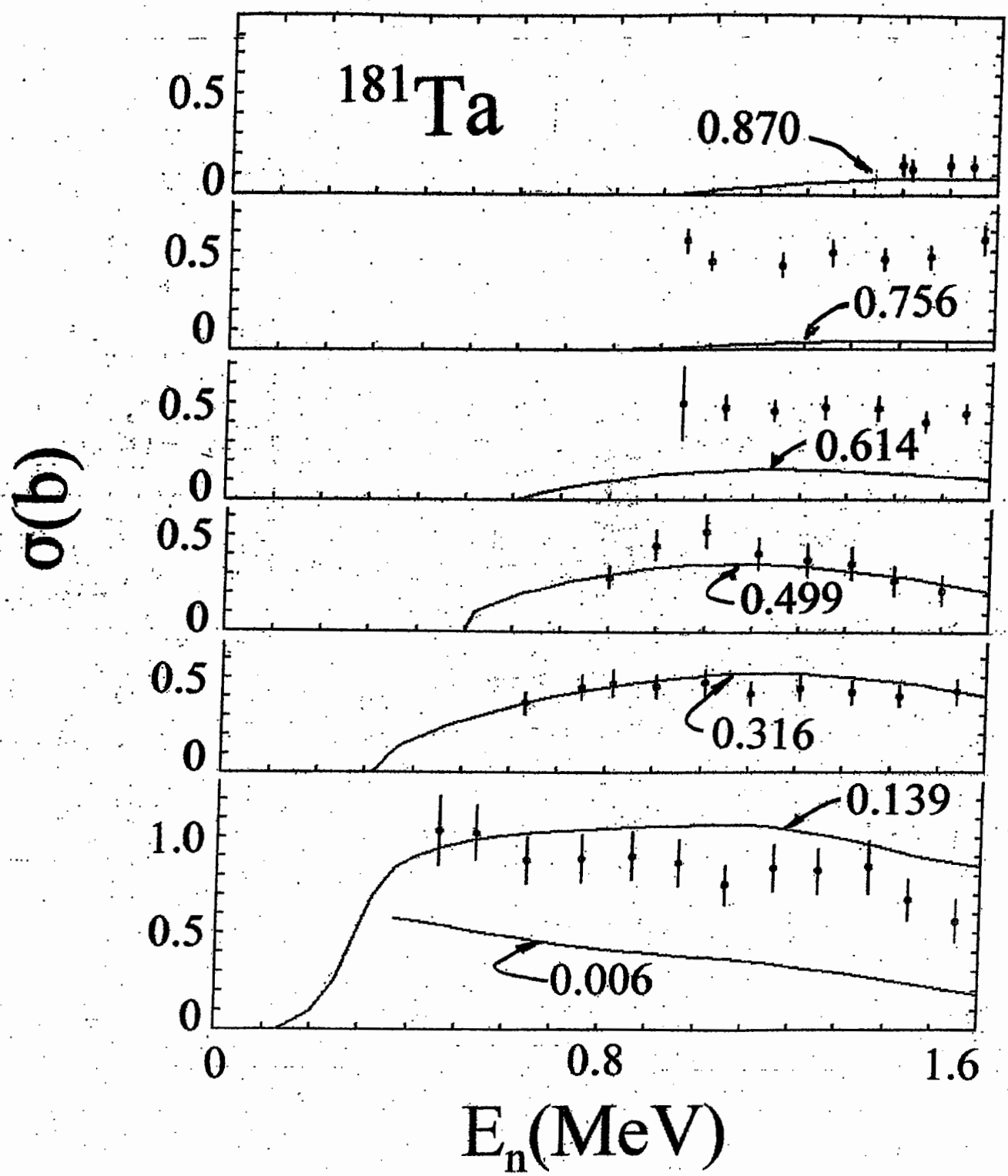

Fig. IV-B-3. Inelastic-excitation cross-sections of tantalum. The present experimental averages are indicated by symbols. The results of calculations using the ROTM of **Table IV-B-1** are denoted by curves. The average experimental excitation energies are numerical given in MeV in each section of the figure. Calculations of the excitation of the unmeasureable 6.2 keV level are also shown for completeness.

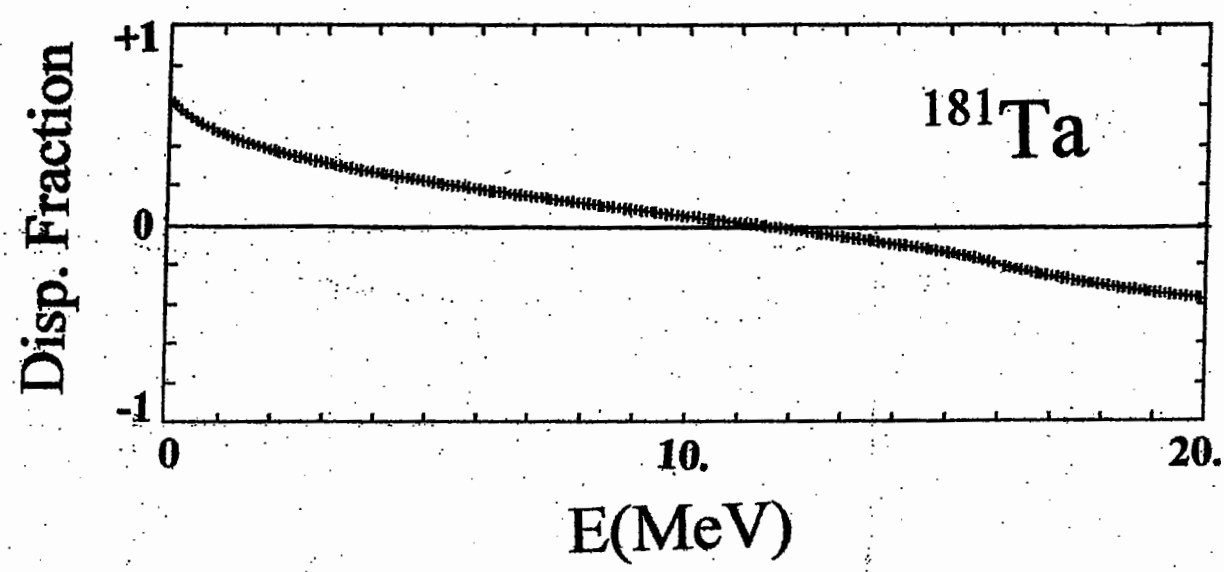

Fig. IV-C-1. Illustrative energy dependence and magnitude of the surface dispersive fraction calculated using the SOM as described in the text. The same qualitative behavior was obtained with the ROTM.

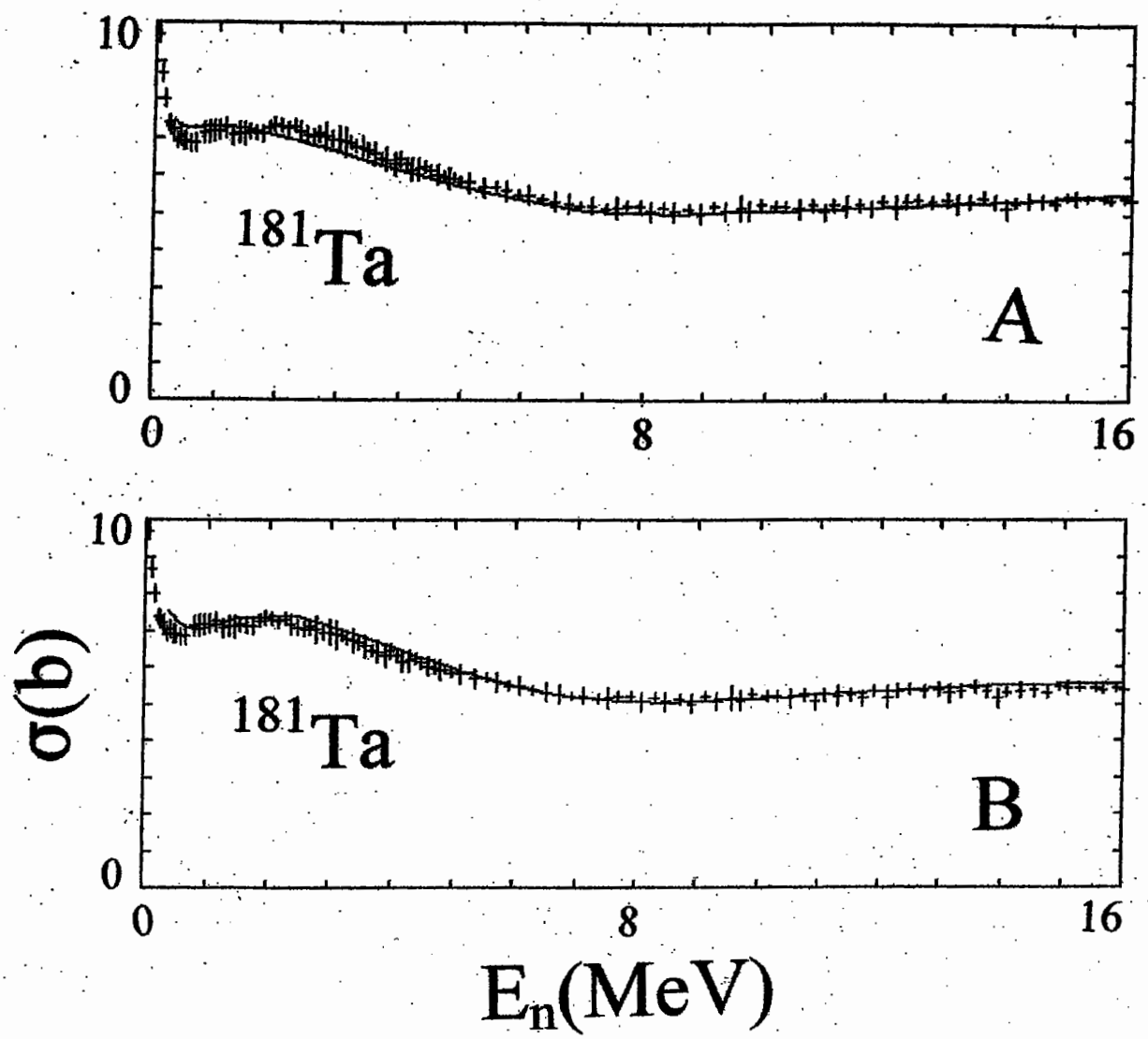

Fig. IV-C-2. Comparison of measured (symbols) and calculated (curves) neutron total cross sections of tantalum. In Panel "A" of the figure the calculations used the Dispersive SOM of **Table IV-C-1**. In Panel "B" the calculations employed the Dispersive ROTM of **Table IV-C-2**.

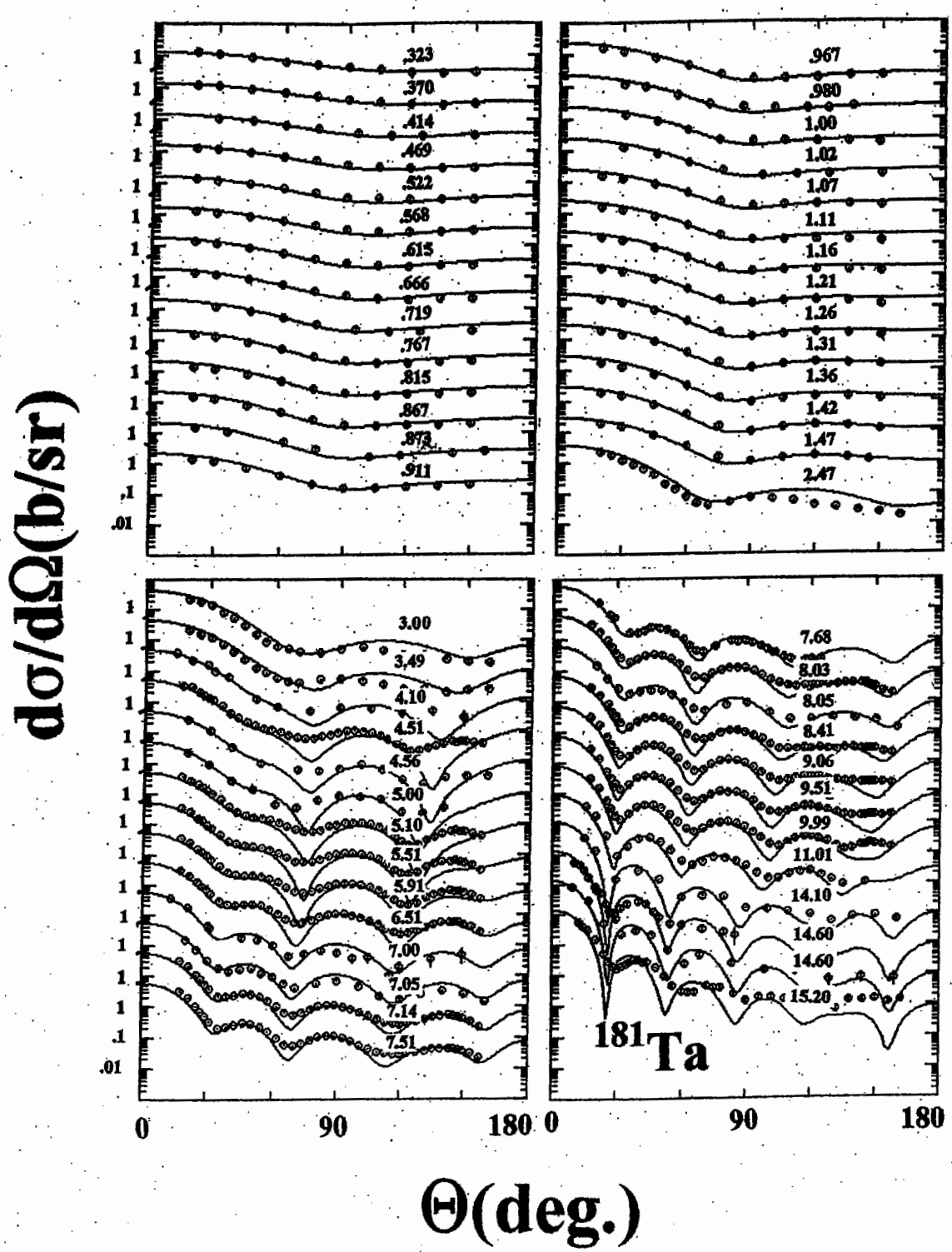

Fig. IV-C-3. Comparisons of measured (symbols) and calculated (curves) differential "elastic" scattering values obtained using the Dispersive SOM of **Table IV-C-1.** The nomenclature is the same as **Fig. IV-A-1**.

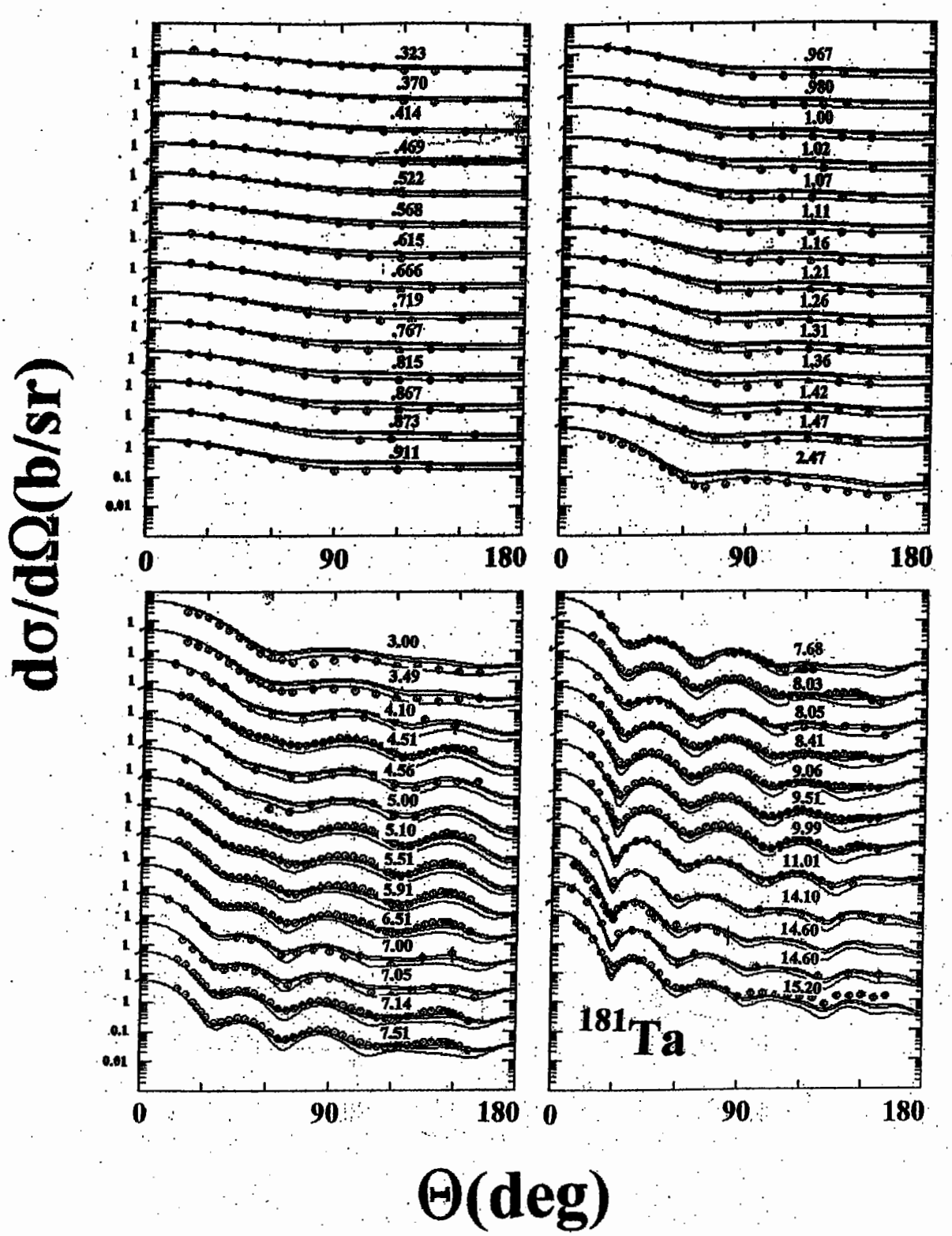

Fig. IV-C-4. Comparisons of measured (symbols) and calculated (curves) differential scattering cross sections obtained using the Dispersive ROTM of **Table IV-C-2.** The nomenclature is the same as in **Fig. IV-B-2.**

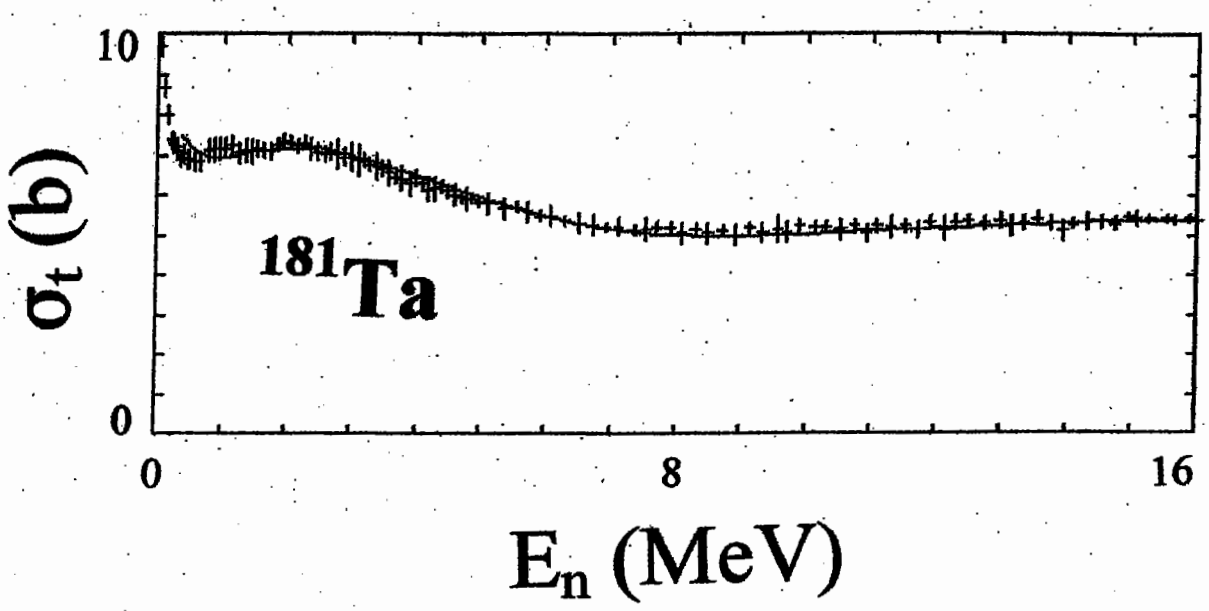

Fig. V-A-1. Comparisons of measured neutron total cross sections of tantalum (symbols) with values calculated with the regional potential of **Table V-A-1(B)** (curve).

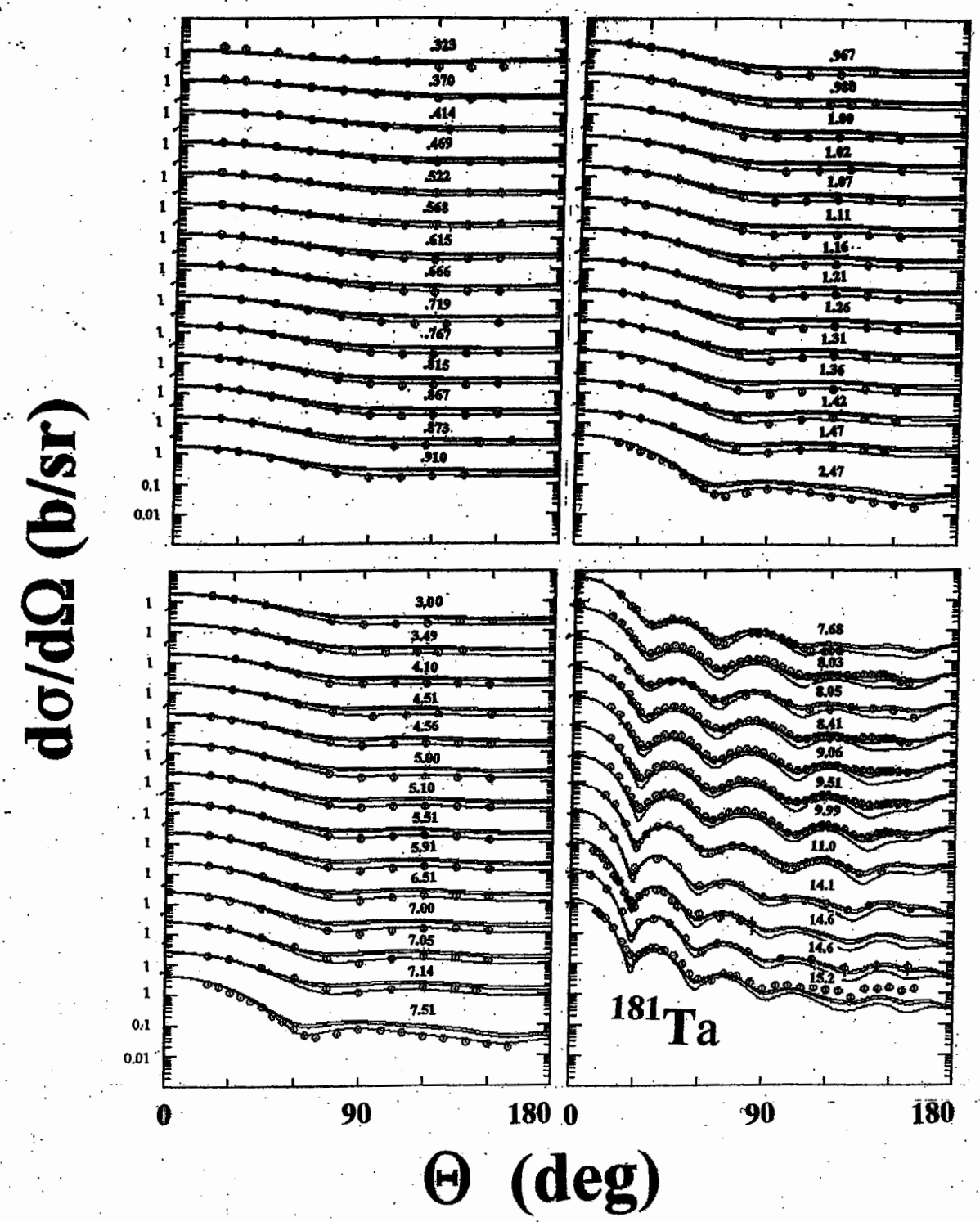

Fig. V-A-2. Comparisons of tantalum differential scattering cross sections calculated with the "regional" potential of **Table V-A-1(B)** (curves) with the experimental values (symbols). The nomenclature of the figure is identical to that of **Fig. IV-B-2**.

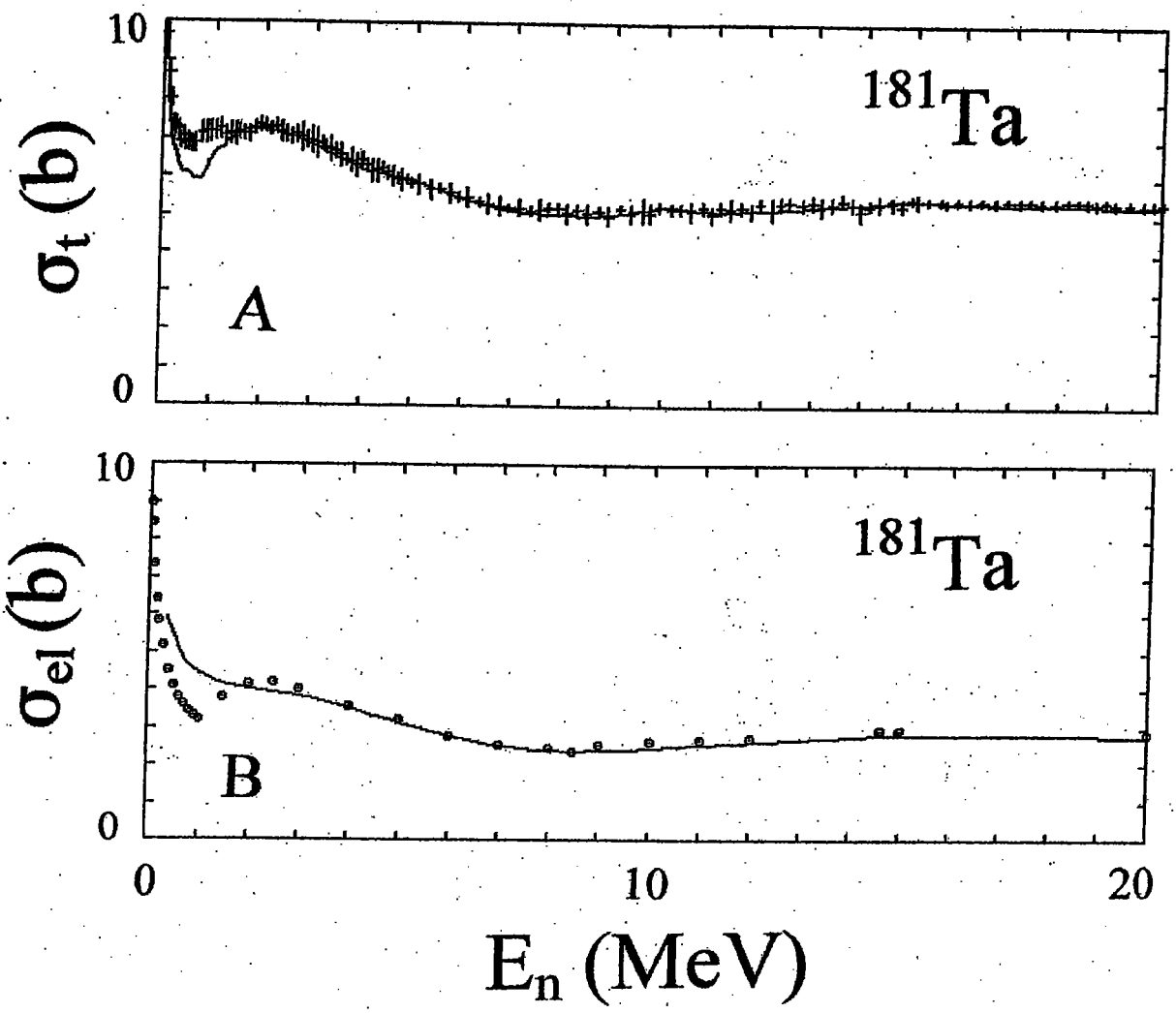

Fig. V-B-1. Comparisons of neutron total and elastic-scattering cross sections of **ENDF/B-VI** with those of the present work. Panel A compares **ENDF/B-VI** total cross sections (curve) and the energy-averaged experimental values of **Appendix A** (symbols). Panel B compares the angle-integrated elastic-scattering cross sections of **ENDF/B_VI** (symbols) with the results of the ROTM calculations (curve) using the potential of **Table-IV-B-1.**

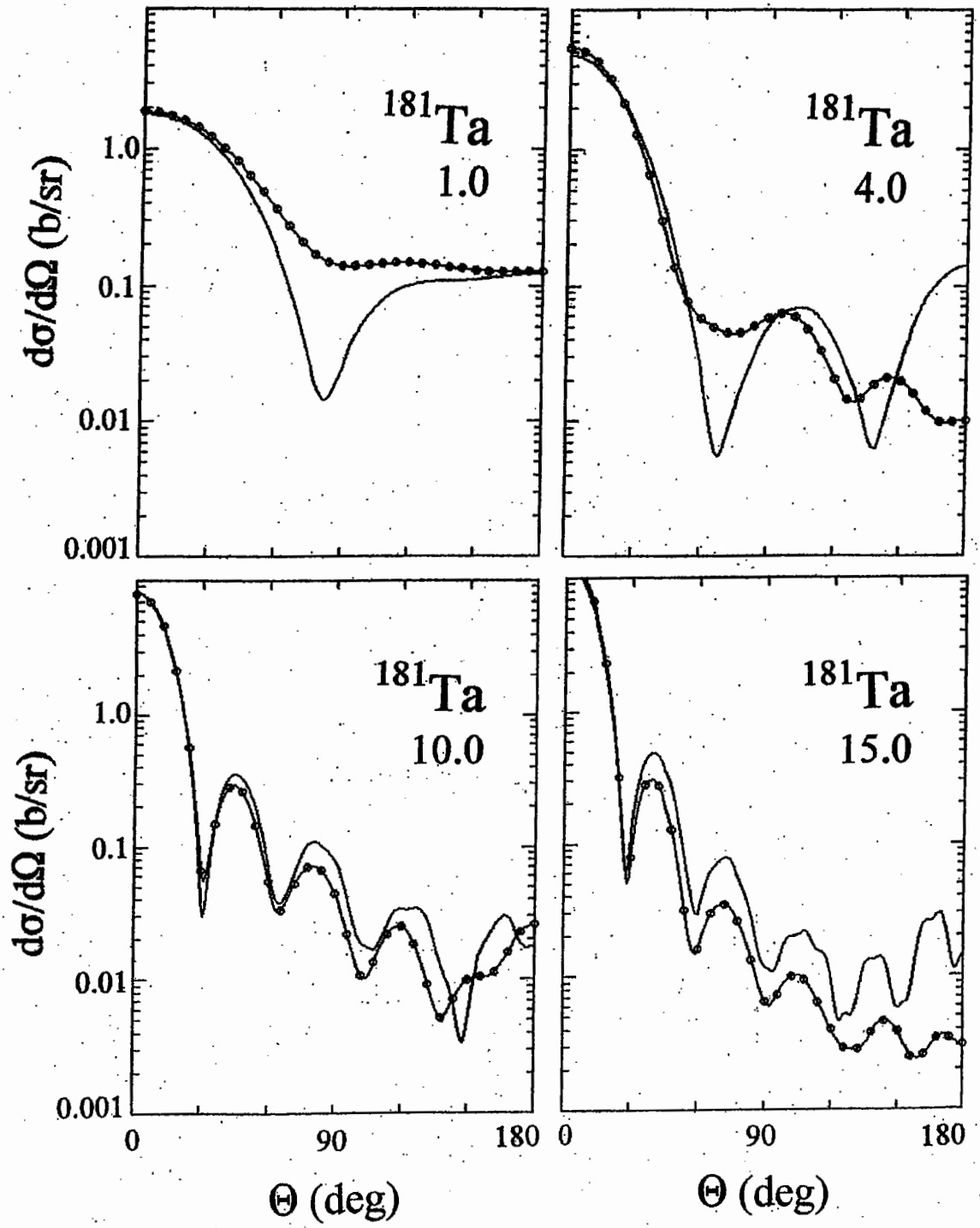

Fig. V-B-2, Representative comparisons of differential elastic-scattering cross sections of tantalum at incident energies of 1.0, 4.0, 10.0 and 15.0 MeV, as numerically noted in each quadrant of the figure. The simple curves denote **ENDF/B-VI** distributions. Curves with circular symbols show the corresponding results obtained with the ROTM of **Sec. IV-B**.

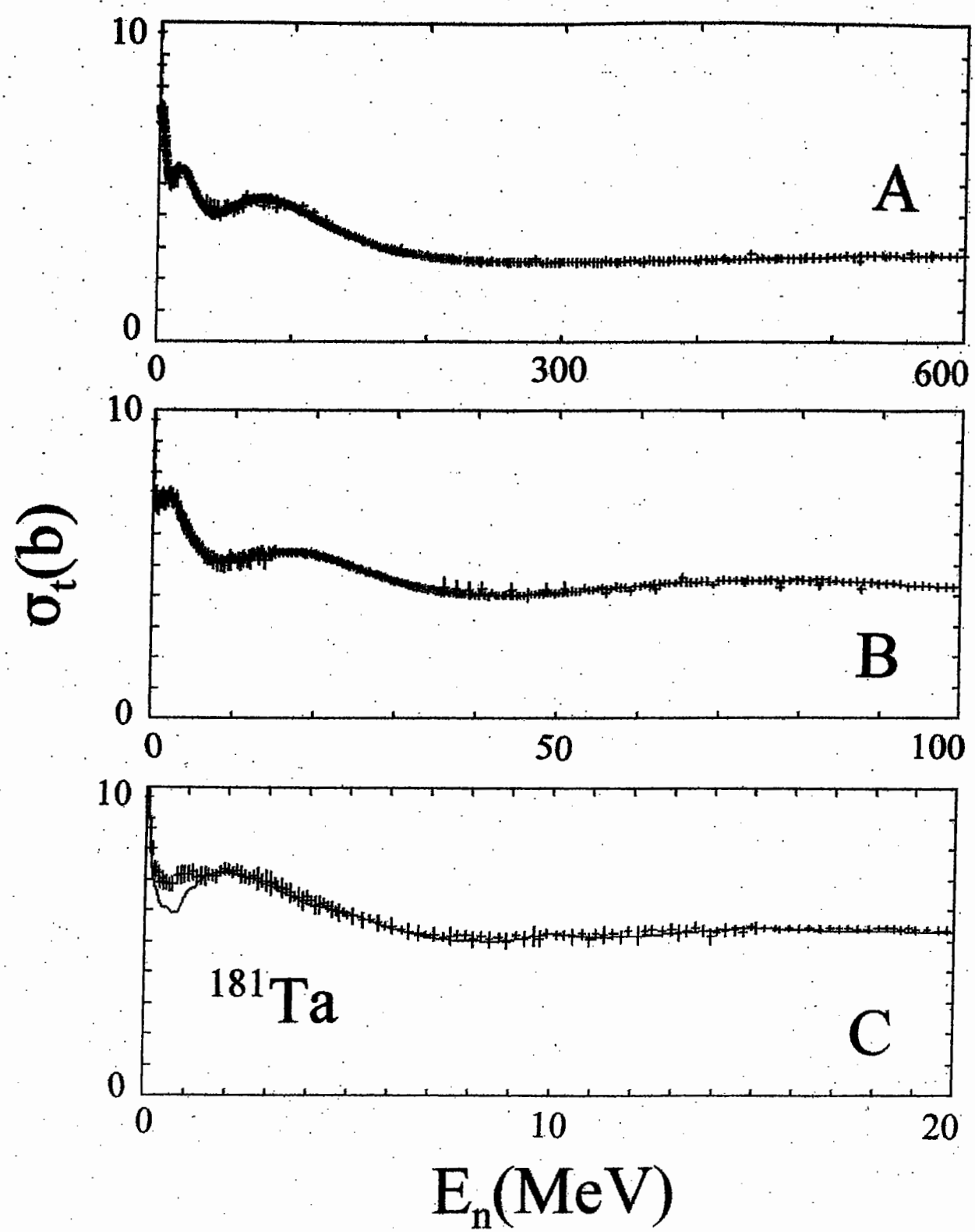

Fig. A-1. Ordered, averaged and combined experimental tantalum neutron total cross sections (symbols), as described in the text of **Appendix A**. All three panels show the same experimental results but on different energy scales, as numerically noted. The curve in Panel C indicates the comparable **ENDF/B-VI** values.